Calibration and measurement uncertainties of a continuous-flow cloud condensation nuclei counter (DMT-CCNC): CCN activation of ammonium sulfate and sodium chloride aerosol particles in theory and experiment

D. Rose, G. P. Frank, U. Dusek, S. S. Gunthe, M. O. Andreae, U. Pöschl

Atmos. Chem. Phys. Discuss., 7, 8193–8260, 2007
www.atmos-chem-phys-discuss.net/7/8193/2007/

Atmospheric Chemistry and Physics Discussions

Calibration and measurement uncertainties of a continuous-flow cloud condensation nuclei counter (DMT-CCNC): CCN activation of ammonium sulfate and sodium chloride aerosol particles in theory and experiment

D. Rose, G. P. Frank, U. Dusek, S. S. Gunthe, M. O. Andreae, and U. Pöschl

Max Planck Institute for Chemistry, Biogeochemistry Department, P.O. Box 3060, 55020 Mainz, Germany

Received: 5 April 2007 – Accepted: 29 May 2007 – Published: 14 June 2007

Correspondence to: D. Rose (rose@mpch-mainz.mpg.de)

Abstract

Experimental and theoretical uncertainties in the measurement of cloud condensation nuclei (CCN) with a continuous-flow thermal-gradient CCN counter from Droplet Measurement Technologies (DMT-CCNC) have been assessed by model calculations and calibration experiments with ammonium sulfate and sodium chloride aerosol particles in the diameter range of 20–220 nm. Experiments have been performed in the laboratory and during field measurement campaigns, extending over a period of more than one year and covering a wide range of operating conditions (650-1020 hPa ambient pressure, 0.5–1.0 L min^{-1} aerosol flow rate, 20–30°C inlet temperature, 4–34 K m^{-1} temperature gradient). For each set of conditions, the effective water vapor supersaturation (S_{eff}) in the CCNC was determined from the measured CCN activation spectra and Köhler model calculations.

High measurement precision was achieved under stable laboratory conditions, where relative variations of S_{eff} in the CCNC were generally less than ±2%. During field measurements, however, the relative variability increased up to ±5–7%, which can be mostly attributed to variations of the CCNC column top temperature with ambient temperature.

To assess the accuracy of the Köhler models used to calculate S_{eff}, we have performed a comprehensive comparison and uncertainty analysis of the various Köhler models and thermodynamic parameterizations commonly used in CCN studies. For the relevant supersaturation range (0.05–2%), the relative deviations between different modeling approaches were as high as 25% for $(NH_4)_2SO_4$ and 16% for NaCl. The deviations were mostly caused by the different parameterizations for the activity of water in aqueous solutions of $(NH_4)_2SO_4$ and NaCl (activity parameterization, osmotic coefficient, and van't Hoff factor models). The uncertainties related to the model parameterizations of water activity clearly exceeded the CCNC measurement precision. Relative deviations caused by different ways of calculating or approximating solution density and surface tension did not exceed 3% for $(NH_4)_2SO_4$ and 1.5%

ACPD

7, 8193–8260, 2007

for NaCl. Nevertheless, they did exceed the CCNC measurement precision under well-defined operating conditions and should not be neglected in studies aimed at high accuracy. To ensure comparability of results, we suggest that CCN studies should always report exactly which Köhler model equations and parameterizations of solution properties were used.

Substantial differences between the CCNC calibration results obtained with $(NH_4)_2SO_4$ and NaCl aerosols under equal experimental conditions (relative deviations of S_{eff} up to ~10%) indicate inconsistencies between widely used activity parameterizations derived from electrodynamic balance (EDB) single particle experiments (Tang and Munkelwitz, 1994; Tang, 1996) and hygroscopicity tandem differential mobility analyzer (HTDMA) aerosol experiments (Kreidenweis et al., 2005). Therefore, we see a need for further evaluation and experimental confirmation of preferred data sets and parameterizations for the activity of water in dilute aqueous $(NH_4)_2SO_4$ and NaCl solutions.

The experimental results were also used to test the CCNC flow model of Lance et al. (2006), which describes the dependence of S_{eff} on temperature, pressure, and flow rate in the CCN counter. This model could be applied after subtraction of a near-constant temperature offset and derivation of an instrument-specific thermal resistance parameter ($R_T \approx 1.8\,K\,W^{-1}$). At $S_{eff} > 0.1\%$ the relative deviations between the flow model and experimental results were mostly less than 5%, when the same Köhler model approach was used. At $S_{eff} \leq 0.1\%$, however, the deviations exceeded 20%, which can be attributed to non-idealities which also caused the near-constant temperature offset. Therefore, we suggest that the CCNC flow model can be used to extrapolate calibration results, but should generally be complemented by calibration experiments performed under the relevant operating conditions – during field campaigns as well as in laboratory studies.

ACPD
7, 8193–8260, 2007

1 Introduction

Aerosol particles serving as cloud condensation nuclei (CCN) play an important role in the formation of clouds and precipitation, and they influence atmospheric chemistry and physics, the hydrological cycle, and climate (Pruppacher and Klett, 1997; Seinfeld and Pandis, 1998; Lohmann and Feichter, 2005). Recent studies indicate that the abundance and properties of CCN may also affect precipitation amount and intensity, heavy weather events and atmospheric dynamics (Andreae et al., 2004; Khain et al., 2005; Rosenfeld and Givati, 2006; Segal and Khain, 2006). The response of cloud characteristics and precipitation processes to increasing anthropogenic aerosol concentrations represents one of the largest uncertainties in the current understanding of climate change (Andreae et al., 2005; IAPSAG, 2007; IPCC, 2007). One of the crucial underlying challenges is to determine the ability of aerosol particles to act as CCN under relevant atmospheric conditions, an issue that has received increasing attention over the past years (McFiggans et al., 2006; IAPSAG, 2007).

The activation of CCN, i.e., the formation of cloud droplets by the condensation of water vapor on aerosol particles, is determined by particle size and composition as well as water vapor supersaturation (Charlson et al., 2001; Segal et al., 2004; Andreae et al., 2005; McFiggans et al., 2006; Andreae et al., 2007).

Reliable measurement data of atmospheric CCN concentration and size distribution as a function of water vapor supersaturation are required for the quantitative description, understanding, and assessment of the effects of natural background aerosols and anthropogenic pollution on the atmosphere and climate. Therefore, CCN measurements have been performed in laboratory and field experiments around the globe, and more are under way (e.g., Gras, 1995; Hudson and Xie, 1999; Delene and Deshler, 2001; Giebl et al., 2002; Hudson and Yum, 2002; Raymond and Pandis, 2003; Bilde and Svenningsson, 2004; Broekhuizen et al., 2004; Dusek et al., 2006; Reade et al., 2006; Roberts et al., 2006; Ervens et al., 2007).

Instruments that measure CCN concentrations at prescribed water vapor

ACPD
7, 8193–8260, 2007

EGU

supersaturations have been available and in use for decades, but the reliability of the measurement results has been a subject of continuing debate (e.g., Hudson, 1989; Hudson, 1993; Chuang et al., 2000; Delene and Deshler, 2000; Snider et al., 2003; Wex et al., 2005; Snider et al., 2006).

Only recently has an instrument promising enhanced robustness and reliability become commercially available: the continuous-flow streamwise thermal-gradient cloud condensation nuclei counter (CCNC) from Droplet Measurement Technologies (DMT). The design and operating principles of the instrument are based on Roberts and Nenes (2005) as detailed below. Numerous atmospheric research groups around the world have recently begun to use instruments of this type for CCN field and laboratory studies.

In this study, we describe how the DMT-CCNC can be efficiently calibrated by experiments using salt aerosol particles of known size and composition, and the corresponding Köhler model calculations. We investigate and quantify the experimental and theoretical uncertainties, and we point out and discuss differences between various widely used Köhler model equations and parameterizations of the relevant thermodynamic properties of ammonium sulfate and sodium chloride in aqueous solution. Moreover, we test the applicability of a CCNC flow model by Lance et al. (2006) for extrapolating DMT-CCNC calibration results to different measurement conditions (temperature, pressure, flow rate).

2 Experimental techniques

2.1 Cloud condensation nuclei counter (CCNC)

The CCNC used and characterized in this study is a continuous-flow streamwise thermal-gradient CCN counter, commercially available from Droplet Measurement Technologies, Inc. (DMT, model No. CCN-2, serial number 02/05/0011). The design and operating principles of the instrument are based on Roberts and Nenes

(2005). The core of the DMT-CCNC is a vertical flow tube of cylindrical shape (inner diameter 2.3 cm, length 50 cm), in which the aerosol sample, surrounded by filtered sheath air (total flow rate Q=0.5–1 L min^{-1}, sheath-to-aerosol flow ratio 10), flows from top to bottom under laminar conditions. The inner surface of the flow tube is continuously wetted, and a linear positive temperature gradient along the flow direction is established and controlled by thermal electric coolers (TEC) and thermocouples, which are mounted at the beginning, middle, and end of the outer wall of the tube (temperatures T_1, T_2, and T_3, respectively). As the laminar flow passes through the column, heat and water vapor are transported from the inner surface towards the center of the tube. Because water molecules diffuse more quickly than heat, a constant water vapor supersaturation is established along the centerline of the column.

The aerosol sample enters the column at the top center of the column, and particles with a critical supersaturation less than the centerline supersaturation are activated as CCN (for definitions of supersaturation and critical supersaturation see Sect. 3.1). The residence time in the column (~6–12 s, depending on flow rate) enables the activated particles to grow into droplets that are sufficiently large (>1 μm) to be detected separately from unactivated particles (usually <<1 μm). An optical particle counter (OPC) at the exit of the column determines the concentration and size distribution of droplets in the size range of 0.75–10 μm. Droplets larger than 1 μm are considered to be activated CCN.

The effective water vapor supersaturation (S_{eff}) in the CCNC is determined by $\Delta T = T_3 - T_1$, which is the temperature difference between the top (T_1, set ~3 K higher than the sample temperature) and the heated bottom of the column (T_3, maximum ~50°C, limited by OPC operating conditions). In this study, ΔT and S_{eff} have been varied in the range of 2–17 K (corresponding to gradients of 4–34 K m^{-1}) and 0.05–1.3%, respectively. Shifting from one supersaturation level to another requires approximately 0.5–3.5 min, depending on the size of the step, and whether it is from lower to higher supersaturations (shorter time) or vice versa (longer time).

ACPD
7, 8193–8260, 2007

2.2 Experimental setup and aerosol generation

The calibration setup used in this study was similar to the one described by Frank et al. (2006b), and is illustrated in Fig. 1. Calibration aerosol was generated by nebulization of an aqueous salt solution (solute mass concentration ~0.01%) of ammonium sulfate ($(NH_4)_2SO_4$, purity >99.5%, supplier: E. Merck, Darmstadt) or sodium chloride (NaCl, purity >99.99%, supplier: Alfa Aesar GmbH & Co KG), using a TSI 3076 Constant Output Atomizer operated with particle-free pressurized air (2.5 bar, 2 L min^{-1}). The polydisperse aerosol was dried to a relative humidity of <15% by dilution with particle-free dry air (~30 L min^{-1}). The excess flow was vented through a filter (HEPA) or into a fume hood/exhaust line, where care was taken to keep overpressure in the system as low as possible (mostly <20 Pa). The dry aerosol (0.5–2 L min^{-1}) was passed through a bipolar charger/radioactive neutralizer (Ni-63, 555 MBq) to establish charge equilibrium, and a differential mobility analyzer (DMA; TSI 3071 Electrostatic Classifier) with closed loop sheath air flow (10 L min^{-1}) was used to select monodisperse particles. To adjust the particle number concentration, the monodisperse aerosol was diluted with particle free air (0–1 L min^{-1}) in a small mixing chamber (glass, ~10 cm^3, built in-house) at the DMA outlet. After dilution, the monodisperse aerosol flow was split into two parallel lines and fed into a condensation particle counter (CPC; TSI 3762; 1 L min^{-1}) and into the CCNC (0.5–1 L min^{-1}). For the calibration experiments, the number concentration of monodisperse aerosol particles was kept below ~3×10^3 cm^{-3} to avoid counting errors caused by coincidence.

2.3 Calibration experiments and data analysis

Determination of 50% activation diameters

In every calibration experiment, the CCNC was operated at five different ΔT values in the range of 2–17 K. For each ΔT, multiple scans were performed, in which the diameter of the dry salt aerosol particles (D) was set to 15 different values in the

range of 18–220 nm. At each D, the number concentration of total aerosol particles (condensation nuclei, CN) was measured with the CPC, and the number concentration of CCN was measured with the CCNC (~60 s waiting time to adjust to the new particle concentration plus 20–30 s averaging time). The activated particle fraction, or CCN efficiency (CCN/CN), was calculated from the averaged concentrations of CN and CCN. From every scan of particle diameters at constant ΔT, we obtained a spectrum of CCN/CN over D ranging from no activation to full activation. The CCN efficiency spectrum was fitted with a cumulative normal distribution function using a nonlinear least-squares fitting routine (Gauss-Newton method, Matlab, MathWorks, Inc.):

$$f_{CCN/CN} = \frac{a}{2}\left(1 + erf\left(\frac{D - D_{50}}{\sigma\sqrt{2}}\right)\right) \quad (1)$$

where erf is the error function, a is the maximum value of $f_{CCN/CN}$, D_{50} is the particle diameter at $f_{CCN/CN}=a/2$, and σ is the standard deviation of the cumulative normal distribution function. Exemplary CCN efficiency spectra and their fits are illustrated in Fig. 2a.

When the DMA selects particles of a given electrical mobility, the particles are not all singly charged. There are also multiply (mostly doubly) charged particles that have the same electrical mobility, but which are larger in diameter. Since the probability of three charges or more is rather low, only doubly charged particles will be mentioned here. Because of their larger diameter, the doubly charged particles activate at a lower supersaturation than the singly charged particles of the same electrical mobility. Therefore, doubly charged particles appear in the activation curve (CCN/CN vs. D) of a chemically homogeneous aerosol as a plateau at smaller diameters (see Figs. 2a and 3). The height of this plateau corresponds to the number fraction of doubly charged particles. It usually becomes larger for larger particle sizes (i.e., smaller supersaturations), because the probability of double charges becomes higher (Wiedensohler, 1988). Furthermore, the height of this plateau depends on the shape of the number size distribution of the generated aerosol particles. The broader the size distribution is, the higher is the concentration of large particles, and the higher

is the fraction of doubly charged particles selected by the DMA. When the fraction of activated doubly charged particles detected among the CCN is high, it is necessary to correct the activation curves for this bias. The effect of this correction on further calculations will be discussed in Sect. 4.1. The correction can be done by calculating the amount of doubly charged particles from the number size distribution of measured aerosol particles assuming a bipolar charge distribution and then subtracting them from the CCN/CN ratio as described in Frank et al. (2006a). An alternative method to fit the activation curves so that only the information from the singly charged particles is used, is to fit the sum of two cumulative Gaussian distribution functions to the measured CCN efficiency spectrum. This method yields 6 fit parameters defined in analogy to Eq. (1) (a_1, a_2, σ_1, σ_2, $D_{50,1}$, $D_{50,2}$). The midpoint of the first, lower distribution function ($D_{50,1}$) can be regarded as the diameter at which half of the doubly charged particles are activated; the midpoint of the second, upper distribution function ($D_{50,2}$) is taken as the diameter at which half of the singly charged particles are activated (D_{50}). However, this technique is only applicable when there are enough data points at the plateau of the doubly charged particles to be fitted. This method also makes the assumption that the fraction of doubly charged particles is constant over the whole size range.

A simpler method to correct the activation curves for doubly charged particles is to determine their fraction from the level of the smaller plateau in the activation curve and to subtract this value from the CCN/CN ratio at each diameter, assuming that the fraction of activated doubly charged particles is constant over the whole particle size range. The activated fraction of singly charged particles can then be calculated as follows:

$$\left.\frac{\mathrm{CCN}}{\mathrm{CN}}\right|_1 = \frac{\mathrm{CCN}_{1+2} - \mathrm{CN}_{1+2} \cdot \left.\frac{\mathrm{CCN}}{\mathrm{CN}}\right|_2}{\mathrm{CN}_{1+2} - \mathrm{CN}_{1+2} \cdot \left.\frac{\mathrm{CCN}}{\mathrm{CN}}\right|_2} \tag{2}$$

In this equation the indices “1” or “2” refer to the fraction of singly or doubly charged particles of a variable. The indices “1+2” describes the measured concentration or fraction consisting of singly and doubly charged particles, respectively. The function

ACPD
7, 8193–8260, 2007

EGU

given in Eq. (1) is fitted to the corrected CCN efficiency spectrum to obtain D_{50}.

Determination of effective supersaturation (S_{eff})

The diameter at which 50% of the monodisperse aerosol particles are activated, i.e., D_{50} as obtained from the fit to the experimental data, can be regarded as the critical dry particle diameter for CCN activation, D_c, i.e., the effective diameter which is required for particles of the given composition to be activated as CCN at the given supersaturation. According to Köhler theory (Sect. 3), D_c can be related to a critical supersaturation, S_c, which is the minimum supersaturation required to activate particles of the given size and composition as CCN, and can be calculated from basic physicochemical parameters of the particle material in aqueous solution. Therefore, Köhler model calculations as detailed in Sect. 3 (model VH4.1 unless mentioned otherwise) were used to derive S_c from D_{50}. S_c can be regarded as the effective water vapor supersaturation in the CCNC (S_{eff}) at the given operating conditions (ΔT, p, T_1, Q).

From each of the multiple CCN efficiency spectra recorded at each of the temperature differences investigated within a calibration experiment, we obtained one data point in a calibration diagram of S_{eff} vs. ΔT. A linear calibration function, $f_s = k_s \Delta T + S_0$, was obtained by a linear least-squares fit to these data points. One exemplary calibration line is illustrated in Fig. 2b. The fit parameters of the calibration function (k_s, S_0) can be used in the CCNC software to calculate and set appropriate temperature differences, ΔT, for CCN measurements at desired water vapor supersaturations, S_{eff}.

2.4 CCNC flow model

Roberts and Nenes (2005) introduced a model that describes the relationship between the temperature difference and S_{eff} in the DMT-CCNC column under certain operating conditions. The input variables to the model are the volumetric flow rate, the sheath-to-aerosol flow ratio, the pressure, and the inner wall streamwise temperature

ACPD
7, 8193–8260, 2007

EGU

difference (ΔT_{inner}) between the exit and the entrance of the column. Lance et al. (2006) compared the simulated instrument responses for calibration aerosol against actual measurements. They indicated that the supersaturation strongly depends on ΔT_{inner} which may be only a fraction of the temperature difference imposed by the TECs at the outer wall of the column ($\Delta T = T_3 - T_1$). It is assumed that the inner temperature at the entrance of the column ($T_{1,inner}$) equals the entrance temperature measured outside the column, i.e., T_1. The temperature drop across the wall – the quotient of ΔT_{inner} to ΔT – is called the thermal efficiency η ($\eta \leq 1$) and varies with the operating conditions. η has to be determined to predict the S_{eff} of the instrument and can be calculated if the thermal resistance (R_T) of the column is known. R_T is a material property and varies between instruments.

Following the procedure suggested by Lance et al. (2006), we calibrated the thermal resistance of our instrument before estimating the thermal efficiency and the supersaturation in the CCNC under different operating conditions. The supersaturation was first determined experimentally by calibrating the CCN counter with ammonium sulfate particles of known size at different ΔT values and inferring S_{eff} by converting the critical diameter into S_c via Köhler theory. The VH4.3 Köhler model (cf. Sect. 3.4) was used to calculate S_c, because the parameters $B_1 - B_5$ of Lance et al. (2006) were based on a van't Hoff factor model with i_s=3. The calibration line (S_{eff} vs. ΔT) did not go through the origin of the coordinate system, but intercepted the x-axis at a certain ΔT_0 (cf. Fig. 2b). Since the model assumes that S=0 if ΔT_{inner}=0 and thus ΔT=0, we shifted the calibration line to the left by subtracting its ΔT_0 from each ΔT, which led to a new calibration line of S_{eff} vs. ΔT^* ($\Delta T^* = \Delta T - \Delta T_0$). Each pair of ΔT^* and S_{eff} was taken to determine ΔT_{inner} by solving Eq. (16) in Lance et al. (2006) iteratively. The thermal efficiency η was calculated dividing ΔT_{inner} by ΔT^*. The thermal resistance R_T, valid for our CCNC unit, was calculated by solving Eq. (15) in Lance et al. (2006).

R_T was used to model the effective supersaturation for any operating condition (T_1, p, Q) of the CCNC. For a given ΔT, ΔT^* was calculated by subtracting a mean value of ΔT_0=1 K and inserted into Eq. (15) in Lance et al. (2006) to calculate η. The inner

wall temperature difference, ΔT_{inner}, was determined by multiplication of η with ΔT^*, and finally, S_{eff} was calculated using Eq. (16) in Lance et al. (2006).

3 Köhler theory and models

In this section, consistent and precise specifications and distinctions of different types of Köhler models frequently used to calculate critical supersaturations for the CCN activation of ammonium sulfate and sodium chloride particles will be presented. Model results and differences will be compared and discussed in Sect. 4.6.

3.1 Basic equations and parameters

According to Köhler theory (Köhler, 1936; Pruppacher and Klett, 1997; Seinfeld and Pandis, 1998), the condition necessary for an aqueous solution droplet to be in equilibrium with water vapor in the surrounding gas phase can be expressed by the following basic equation (Kreidenweis et al., 2005; Koehler et al., 2006):

$$s = a_w \cdot Ke \tag{3}$$

The water vapor saturation ratio, s, is defined as the ratio of the actual partial pressure of water to the equilibrium vapor pressure over a flat surface of pure water at the same temperature. Expressed in percent, s is identical to the relative humidity (RH), which is typically used to describe the abundance of water vapor under sub-saturated conditions. Under supersaturated conditions (s>1, RH>100%), it is customary to describe the abundance of water vapor by the so-called supersaturation S, which is expressed in percent and defined by:

$$S = (s - 1) \cdot 100\,\% \tag{4}$$

a_w is the activity of water in the aqueous solution, and Ke is the so-called Kelvin term, which describes the enhancement of the equilibrium water vapor pressure due to surface curvature.

Under the common assumption that the partial molar volume of water can be approximated by the molar volume of pure water (Kreidenweis et al., 2005), the Kelvin term for a spherical aqueous solution droplet with the diameter D_{wet} is given by:

$$Ke = \exp\left(\frac{4\,\sigma_{sol}\,M_w}{R\,T\,\rho_w\,D_{wet}}\right) \quad (5)$$

M_w and ρ_w are the molar mass and density of water, and σ_{sol} is the surface tension of the solution droplet. R and T are the universal gas constant and absolute temperature, respectively. Deviations from this approximation are generally negligible for the dilute aqueous solution droplets formed by hygroscopic salts like ammonium sulfate and sodium chloride at $s \approx 1$ (Brechtel and Kreidenweis, 2000; Kreidenweis et al., 2005). To describe a_w and σ_{sol} as a function of droplet composition, various types of equations, parameterizations, and approximations have been proposed and can be used as detailed below.

For a given type and mass of solute (dissolved substance), a plot of s vs. D_{wet} generally exhibits a maximum in the region where $s>1$ and $S>0$. The saturation ratio and supersaturation at this maximum are the so-called critical saturation s_c and critical supersaturation S_c, respectively, which are associated with the so-called critical droplet diameter, $D_{wet,c}$. Droplets reaching or exceeding this diameter can freely grow by condensation of water vapor from the supersaturated gas phase and form cloud droplets (Pruppacher and Klett, 1997; Seinfeld and Pandis, 1998).

Aerosol particles consisting of soluble and hygroscopic substances, such as ammonium sulfate and sodium chloride, generally take up water vapor and already form aqueous solution droplets at $s<1$ (hygroscopic growth). The ratio of the droplet diameter, D_{wet}, to the diameter of a compact spherical particle consisting of the dry solute, D_s (mass equivalent diameter of the dry solute particle), is defined as the (mass equivalent) growth factor of the dry solute particle, g_s:

$$g_s = \frac{D_{wet}}{D_s} = \left(\frac{\rho_s}{x_s \rho_{sol}}\right)^{\frac{1}{3}} \quad (6)$$

x_s is the mass fraction of the solute in the droplet, and ρ_s is the density of the dry solute (cf. Table 1). Equations (3), (5), and (6) can be used to describe the hygroscopic growth and CCN activation of aerosol particles (D_{wet} as a function of s – or vice versa – for any given value of D_s), if a_w, ρ_{sol}, and σ_{sol} are known as a function of droplet composition, which is usually described by the solute mass fraction x_s, molality μ_s, or molarity c_s.

The molality is defined as the amount of substance (number of moles) of solute, $n_s{=}m_s M_s^{-1}$, divided by the mass of solvent, i.e., by the mass of water in an aqueous solution, $m_w{=}n_w M_w$. M_s is the molar mass of the solute (cf. Table 1), m_s is the mass of the solute, and n_w is the amount of substance (number of moles) of water in the solution.

The molarity is defined as the amount of substance divided by the volume of the solution in units of mol L^{-1}. Mass fraction, molality, and molarity of the solute are related by:

$$\mu_s = \frac{x_s}{M_s\,(1-x_s)} = \frac{m_s}{M_s\,m_w} = \frac{n_s}{M_w\,n_w} = \frac{\pi\,\rho_s\,D_s^3}{6\,M_s\,n_w\,M_w} \tag{7}$$

$$c_s = \frac{x_s\,\rho_{\mathrm{sol}}}{M_s} \cdot 10^{-3}\mathrm{m}^3\,\mathrm{L}^{-1} \tag{8}$$

The scaling factor $10^{-3}\,\mathrm{m}^3\,\mathrm{L}^{-1}$ is required to relate the molarity in mol L^{-1} to the other quantities, which are generally given in SI units.

Depending on the types of parameterizations used to describe a_w, ρ_{sol}, and σ_{sol}, different models can be used to calculate the critical supersaturation S_c for any given value of D_s. The different options considered and compared in this study are outlined below and discussed in Sect. 4.6.

In the Köhler model calculations used for CCNC calibration, the experimentally determined critical dry particle diameter D_c (i.e., the fit parameter D_{50}, or a shape corrected value as detailed in Sect. 3.6) was taken as the dry solute mass equivalent

diameter D_s, corresponding to a solute mass of $m_s = \pi/6\,\rho_s\,D_s^3$. The CCNC column top temperature (T_1) was taken as the model temperature T.

3.2 Activity parameterization (AP) models

For the activity of water in aqueous solution droplets of $(NH_4)_2SO_4$, NaCl, and other salts, Tang and Munkelwitz (1994) and Tang (1996) have presented parameterizations derived from electrodynamic balance (EDB) single particle experiments as polynomial fit functions of solute mass percentage ($100\,x_s$):

$$a_w = 1 + \sum_q a_q\,(100\,x_s)^q \tag{9}$$

The polynomial coefficients a_q for $(NH_4)_2SO_4$ and NaCl at 298 K are listed in Table 2.

An alternative parameterization of a_w has been proposed by Kreidenweis et al. (2005), who derived the following relation between a_w and the growth factor of dry solute particles (g_s) determined in measurements with a hygroscopicity tandem differential mobility analyzer (HTDMA):

$$g_s = \frac{D_{\text{wet}}}{D_s} = \left(1 + \left(k_a + k_b \cdot a_w + k_c \cdot a_w^2\right)\frac{a_w}{1 - a_w}\right)^{\frac{1}{3}} \tag{10}$$

The coefficients k_a, k_b, and k_c for $(NH_4)_2SO_4$ and NaCl are listed in Table 2.

Low (1969) provided a table of a_w for ammonium sulfate and sodium chloride for molalities of 0.1–6 mol kg^{-1}. For the calculation of S_c, however, this range of molalities is insufficient and has to be extrapolated below 0.1 mol kg^{-1}. We have tested this approach with a third order polynomial fit, but the results were very different from the parameterizations given above (deviations up to a factor of 2 in S_c) and are not discussed any further.

For the density of aqueous solution droplets of $(NH_4)_2SO_4$, NaCl, and other salts, Tang and Munkelwitz (1994) and Tang (1996) have also presented parameterizations

ACPD
7, 8193–8260, 2007

EGU

of experimentally determined values as polynomial fit functions of solute mass percentage ($100\ x_s$):

$$\rho_{sol} = \rho_w + \left[\sum_q d_q\ (100\, x_s)^q\right] \cdot 10^3\,\mathrm{kg\,m^{-3}} \tag{11}$$

ρ_w is the density of pure water in $\mathrm{kg\,m^{-3}}$ (e.g., $997.1\,\mathrm{kg\,m^{-3}}$ at 298 K) and the coefficients for $(NH_4)_2SO_4$ and NaCl at 298 K are listed in Table 3.

Under the assumption of volume additivity (partial molar volumes of solute and solvent in solution are equal to molar volumes of pure substances; Mikhailov et al., 2004), ρ_{sol} can also be calculated by

$$\rho_{\mathrm{sol}} = \left(\frac{1 - x_s}{\rho_w} + \frac{x_s}{\rho_s}\right)^{-1} \tag{12}$$

The simplest parameterization of ρ_{sol} used in this study was approximating it by the density of pure water, either with a constant value of $997.1\,\mathrm{kg\,m^{-3}}$ or a temperature dependent one. The temperature dependence of the density of pure water can be described by Pruppacher and Klett (1997):

$$\rho_w = \frac{A_0 + A_1 t + A_2 t^2 + A_3 t^3 + A_4 t^4 + A_5 t^5}{1 + Bt} \tag{13}$$

Here t is the temperature in °C (t=T–273.15 K) and A_0=999.8396 $\mathrm{kg\,m^{-3}}$, A_1=18.224944 $\mathrm{kg\,m^{-3}\,°C^{-1}}$, A_2=-7.92221×10^{-3} $\mathrm{kg\,m^{-3}\,°C^{-2}}$, A_3=-55.44846×10^{-6} $\mathrm{kg\,m^{-3}\,°C^{-3}}$, A_4=149.7562×10^{-9} $\mathrm{kg\,m^{-3}\,°C^{-4}}$, A_5=-393.2952×10^{-12} $\mathrm{kg\,m^{-3}\,°C^{-5}}$, and B=18.159725×10^{-3} $\mathrm{°C^{-1}}$.

The deviations caused by using different parameterizations and approximations of ρ_{sol} turned out to be small, as will be detailed below (Sect. 4.6).

For the surface tension of aqueous salt solution droplets, Seinfeld and Pandis (1998) proposed the following parameterization:

$$\sigma_{\mathrm{sol}} = \sigma_w + \gamma_s \cdot c_s \tag{14}$$

in which γ_s=2.17×10^{-3} N m^{-1} L mol^{-1} for $(NH_4)_2SO_4$ and γ_s=1.62×10^{-3} N m^{-1} L mol^{-1} for NaCl. σ_w is the surface tension of pure water as detailed below, and c_s is the molarity of the solute. Alternative concentration-dependent parameterizations (Hänel, 1976; Weast and Astle, 1982; Chen, 1994; Gysel et al., 2002) exhibited only small deviations in σ_w in the concentration range of interest (<1% for μ_s<1 mol kg^{-1}).

The simplest parameterization of σ_{sol} used in this study was approximating it by the surface tension of pure water, either with a constant value of 0.072 N m^{-1} or a temperature dependent one. According to Seinfeld and Pandis (1998), the temperature dependence of the surface tension of pure water can be described by:

$$\sigma_w = 0.0761\,\mathrm{N\,m^{-1}} - 1.55\times10^{-4}\,\mathrm{N\,m^{-1}\,K^{-1}}\,(T-273\,\mathrm{K}) \quad (15)$$

Combination of Eqs. (3), (5), and (6) leads to the following version of the Köhler equation, which was taken as the basis for all activity parameterization (AP) model calculations:

$$s = a_w \exp\left(\frac{4\,\sigma_{sol}\,M_w}{\rho_w\,R\,T\,g_s\,D_s}\right) \quad (16)$$

Depending on the applied type of water activity parameterization, we distinguish two types of AP models: AP1 using the mass percentage-based parameterizations of Tang and Munkelwitz (1994) and Tang (1996), and AP2 using the growth factor-based parameterizations of Kreidenweis et al. (2005).

In AP1 model calculations, x_s was taken as the primary variable to calculate a_w from Eq. (9); ρ_{sol} from Eq. (11) with ρ_w from Eq. (13); g_s from Eq. (6); σ_{sol} from Eq. (14) with σ_w from Eq. (15) and c_s from Eq. (8); and s from Eq. (16) (base case AP1.1, Table 5). The maximum value of s (critical saturation ratio, s_c) was determined by the variation of x_s (numerical minimum search for $-s$ with the 'fminsearch' function, Matlab software), and via Eq. (4) it was converted into the corresponding critical supersaturation S_c. In sensitivity studies investigating the influence of various simplifications and approximations of the droplet density and surface tension, individual parameterizations

were exchanged as detailed in Table 5, but the basic calculation procedure remained unchanged (test cases AP1.2-AP1.5).

In AP2 model calculations, a_w was taken as the primary variable to calculate g_s from Eq. (10); ρ_{sol} from Eq. (12) with ρ_w from Eq. (13); $x_s = m_s/(m_s+m_w)$, and $m_w = \pi/6\,\rho_w\,D_s^3\left(g_s^3 - 1\right)$ (volume additivity assumption); σ_{sol} from Eq. (14) with σ_w from Eq. (15) and c_s from Eq. 8; and s from Eq. (16) (base case AP2, Table 5). The maximum value of s (critical saturation ratio) was determined by variation of a_w (numerical minimum search for $-s$ with the 'fminsearch' function, Matlab software), and via Eq. (4) it was converted into the corresponding S_c.

3.3 Osmotic coefficient (OS) models

According to Robinson and Stokes (1959), the activity of water in aqueous solutions of ionic compounds can be described by:

$$a_w = \exp\left(-\nu_s\,\Phi_s\,\mu_s\,M_w\right) \tag{17}$$

ν_s is the stoichiometric dissociation number of the solute, i.e., the number of ions per molecule or formula unit ($\nu_{NaCl}=2$, $\nu_{(NH_4)_2SO_2}=3$). Φ_s is the molal or practical osmotic coefficient of the solute in aqueous solution, which deviates from unity if the solution is not ideal (incomplete dissociation, ion-ion and ion-solvent interactions).

Based on an ion-interaction approach, Pitzer and Mayorga (1973) derived semiempirical parameterizations, which describe Φ_s as a function of solute molality μ_s. The general form for electrolytes dissociating into two types of ions is:

$$\Phi_s = 1 - |z_1 z_2|\left(A_\Phi \frac{\sqrt{I}}{1+b\sqrt{I}}\right) + \mu_s \frac{2\nu_1\nu_2}{\nu_s}\left(\beta_0 + \beta_1 e^{-\alpha\sqrt{I}}\right) + \mu_s^2 \frac{2\,(\nu_1\nu_2)^{\frac{2}{3}}}{\nu_s} C_\Phi \tag{18}$$

ν_1 and ν_2 are the numbers of positive and negative ions produced upon dissociation per formula unit of the solute ($\nu_s=\nu_1+\nu_2$); z_1 and z_2 are the numbers of elementary charges carried by the ions ($(NH_4)_2SO_4$ $\nu_1=z_2=2$ and $\nu_2=z_1=1$; NaCl $\nu_1=\nu_2=z_1=z_2=1$). The

ionic strength is given by I=0.5 μ_s (ν_1 z_1^2 + ν_2 z_2^2). A_Φ is the Debye-Hückel coefficient which has the value 0.3915 (kg mol^{-1})$^{1/2}$ for water at 298.15 K. The parameters α and b are 2 (kg mol^{-1})$^{1/2}$ and 1.2 (kg mol^{-1})$^{1/2}$, respectively. The coefficients β_0, β_1 and C_Φ depend on the chemical composition of the solute and have been tabulated by Pitzer and Mayorga (1973) for over 200 compounds (1:1, 1:2, and 2:1 electrolytes). For ammonium sulfate and sodium chloride, at 298.15 K, the respective values and more recent updates from Mokbel et al. (1997) are listed in Table 4. The OS model calculations were performed in analogy to the AP1 model calculations as detailed above (with x_s as the primary variable for the calculation of other parameters), except that a_w was calculated from Eq. (17) with Φ_s from Eq. (18) and μ_s from Eq. (7).

3.4 Van't Hoff factor (VH) models

According to McDonald (1953) and the early cloud physics literature, the activity of water in aqueous solutions of ionic compounds can be described by the following form of Raoult's law, where the effects of ion dissociation and interactions are represented by the so-called van't Hoff factor, i_s:

$$a_w = \frac{n_w}{n_w + i_s n_s} = \left(1 + i_s \frac{n_s}{n_w}\right)^{-1} = (1 + i_s \mu_s M_w)^{-1} \quad (19)$$

For strong electrolytes such as ammonium sulfate and sodium chloride, the van't Hoff factor is similar to the stoichiometric dissociation number, and deviations of i_s from ν_s can be attributed to solution non-idealities (incomplete dissociation, ion-ion and ion-solvent interactions). The exact relation between i_s and ν_s or Φ_s is given by equating Eqs. (17) and (19). As detailed by Kreidenweis et al. (2005), the resulting equation can be approximated by a series expansion of the exponential term in Eq. (17), inserting n_s/n_w=$\mu_s M_w$ (cf. Eq. 7) and truncation of the series. It follows then that:

$$i_s \approx \nu_s \Phi_s \quad (20)$$

Deviations from this approximation are negligible for the dilute aqueous solution droplets formed by hygroscopic salts such as ammonium sulfate and sodium chloride at $s \approx 1$ (molalities <0.01 mol kg^{-1}; relative magnitude of quadratic and higher terms of series expansion <1%).

Combination of Eqs. (16) and (17) with $\mu_s = m_s/(M_s\, m_w)$, $m_w = \pi/6\, D_{\mathrm{wet}}^3\, \rho_{\mathrm{sol}} - m_s$, $g_s\, D_s = D_{\mathrm{wet}}$, and $i_s \approx \nu_s\, \Phi_s$ leads to:

$$s = \exp\left(\frac{4\,\sigma_{\mathrm{sol}}\, M_w}{\rho_w\, R\, T\, D_{\mathrm{wet}}} - \frac{i_s\, m_s\, M_w}{M_s\left(\pi/6 D_{\mathrm{wet}}^3\, \rho_{\mathrm{sol}} - m_s\right)}\right) \tag{21}$$

For the dilute aqueous solution droplets formed by hygroscopic salts like ammonium sulfate and sodium chloride at $s \approx 1$, the contribution of the solute to the total mass of the droplet is low ($m_s/(\pi/6\, D_{\mathrm{wet}}^3\, \rho_{\mathrm{sol}})$<4% at D_s=20 nm and <0.1% at 200 nm). If m_s is neglected, Eq. (21) reduces to:

$$s = \exp\left(\frac{4\,\sigma_{\mathrm{sol}}\, M_w}{\rho_w\, R\, T\, D_{\mathrm{wet}}} - \frac{6\, i_s\, m_s\, M_w}{\pi\, M_s\, D_{\mathrm{wet}}^3\, \rho_{\mathrm{sol}}}\right) \tag{22}$$

For the dilute salt solution droplets, differences between ρ_w and ρ_{sol} (<3% at D_s=20 nm, <0.1% at 200 nm) and between σ_{sol} and σ_w (<1% at D_s=20 nm, ~0% at 200 nm) are also relatively small. With the approximations of $\rho_{\mathrm{sol}} \approx \rho_w$ and $\sigma_{\mathrm{sol}} \approx \sigma_w$, Eq. (22) can be transformed into the following simplified and widely used form of the Köhler equation (e.g., Pruppacher and Klett, 1997; Seinfeld and Pandis, 1998):

$$s = \exp\left(\frac{A}{D_{\mathrm{wet}}} - \frac{B}{D_{\mathrm{wet}}^3}\right) \tag{23}$$

where

$$A = \frac{4\,\sigma_w\, M_w}{\rho_w\, R\, T} \tag{24}$$

and

$$B = \frac{6\, i_s\, m_s\, M_w}{\pi\, M_s\, \rho_w} = \frac{i_s\, M_w\, \rho_s\, D_s^3}{M_s\, \rho_w} = \frac{6\, i_s\, n_s\, M_w}{\pi\, \rho_w} \tag{25}$$

Under the assumption of complete dissociation and ideal solution behavior (Φ_s=1), the van't Hoff factor is i_s=2 for NaCl and i_s=3 for $(NH_4)_2SO_4$ solutions. For NaCl this approximation is quite common and the deviations from experimental results are small (Gerber et al., 1977), but for $(NH_4)_2SO_4$ it has been shown that i_s has to be between 2 and 2.5 to achieve agreement between measured and calculated droplet diameters (Gerber et al., 1977; Pradeep Kumar et al., 2003).

McDonald (1953) already remarked that the van't Hoff factor is not a constant value, but varies with the solute molality. Low (1969) presented a table of van't Hoff factors for a number of electrolytes at molalities of 0.1–6 mol kg^{-1} and 25°C. For ammonium sulfate, $i_s(\mu_s)$ can be parameterized with the following cubic polynomial fit of the tabulated values (cf. Frank et al., 2006b):

$$i_{s,\mathrm{Low}} = 0.021\,\mathrm{kg^2\,mol^{-2}} \cdot \mu_s^2 - 0.0428\,\mathrm{kg\,mol^{-1}} \cdot \mu_s + 1.9478 \tag{26}$$

The van't Hoff factor for ammonium sulfate was also parameterized by Young and Warren (1992):

$$i_{s,Y\&W} = -0.007931 \cdot \log\left(\mu_s \cdot \mathrm{kg\,mol^{-1}}\right)^2 - 0.1844 \cdot \log\left(\mu_s \cdot \mathrm{kg\,mol^{-1}}\right) + 1.9242 \tag{27}$$

which is also valid for smaller molalities.

Four different VH model calculations were done using the different Köhler equations given in this chapter.

The non-simplified VH model calculations (VH1) for ammonium sulfate solution droplets were made taking μ_s as the primary variable to calculate a_w from Eq. (19) and to calculate i_s. The value of i_s was calculated from Eq. (26) for μ_s>1, and from Eq. (27) for $\mu_s \leq 1$ as suggested by Frank et al. (2006b). $x_s = m_s/(m_s+m_w)$, and m_w

were calculated from Eq. (7); ρ_{sol} from Eq. (11) with ρ_w from Eq. (13); g_s from Eq. (6); σ_{sol} from Eq. (14) with σ_w from Eq. (15) and c_s from Eq. (8); and s from Eq. (16).

VH2 model calculations were made using a simplified Köhler equation (Eq. 21; assuming $i_s \approx \nu_s \Phi_s$). In this equation, i_s was calculated as in VH1 using μ_s as a primary variable. x_s, ρ_w, ρ_{sol}, and σ_{sol} were calculated as in VH1. D_{wet} was calculated from Eq. (6).

A further simplified Köhler equation (Eq. 22) was used to make VH3 model calculations. μ_s was taken as a primary variable to calculate i_s. i_s, x_s, ρ_w, ρ_{sol}, and σ_{sol} were calculated as in VH1; D_{wet} as in VH2; all parameters were inserted into Eq. (22) to calculate s.

The VH4 model used Eq. (23) to calculate s. μ_s was taken as a primary variable to calculate i_s. i_s, x_s, ρ_w, σ_w were calculated as in VH1. D_{wet} was calculated from Eq. (6) which required the parameterization of ρ_{sol}. Because the Köhler equation used for VH4 was derived assuming ρ_{sol} as ρ_w, the same approximation was also used to calculate D_{wet}.

For all VH model calculations, the maximum value of s was determined by variation of μ_s (numerical minimum search for $-s$ with the 'fminsearch' function, Matlab software). The critical supersaturation S_c was calculated from the maximum of s using Eq. (4).

In sensitivity studies investigating the influence of simplifications and approximations, individual parameterizations were exchanged as detailed in Table 5, but the basic calculation procedure (VH1.1, VH2.1, VH3.1, VH4.1) remained unchanged.

3.5 Analytical approximation (AA) model

In all Köhler model calculations that have been presented so far, the critical saturation s_c was determined through numerical iteration by varying the primary variable (such as μ_s, x_s, or a_w) for s in the particular proposed equation until it reached a maximum. Assuming a concentration-independent van't Hoff factor, the iterative numerical solution can be approximated by a simplified analytical equation expressing s_c as a function of

dry solute particle mass equivalent diameter, D_s (Seinfeld and Pandis, 1998):

$$s_c = \exp\left(\sqrt{\frac{4A^3}{27B}}\right) = \exp\left(\sqrt{\frac{4A^3 M_s \rho_w}{27\, i_s M_w \rho_s D_s^3}}\right) \quad (28)$$

In the AA model calculations presented below, the widely used approximation $A \cong 0.66\,\mathrm{K}/T$ was inserted for the Kelvin term parameter A as defined in Eq. (24) (Seinfeld and Pandis, 1998) and different van't Hoff factors were tested (i_s=2.2 or 3 for ammonium sulfate; i_s=2 for sodium chloride).

A comparison and discussion of critical supersaturations calculated with the different AP, OS, VH, and AA models specified above is given in Sect. 4.6. Unless mentioned otherwise the VH4.1 model has been used for CCNC calibration.

3.6 Particle shape corrections

Sodium chloride particles generated by nebulization of a NaCl solution and subsequent drying are usually of cubic shape (Scheibel and Porstendörfer, 1983; Krämer et al., 2000; Mikhailov et al., 2004). In a DMA, the particle size is selected according to the electrical mobility diameter, which assumes a spherical shape of the particles. In the case of cubic particles the diameter selected by the DMA would be overestimated by 4–5% which would thus result in an underestimation of the calculated S_c. Therefore, it is necessary for the diameter to be corrected for the particle shape, which can be done as described, e.g., in Krämer et al. (2000). A shape factor χ is introduced, which is defined as the ratio of the drag force experienced by the particle in question to that of a sphere of equivalent mass:

$$\chi = \frac{D_B\, C\,(D_m)}{D_m\, C\,(D_B)} \quad (29)$$

D_B is the mobility equivalent diameter of the particle, i.e., the diameter which is selected by the DMA, D_m is the mass equivalent diameter, i.e., the corrected diameter which

has to be used for further Köhler model calculations, and $C(D_B)$ and $C(D_m)$ are the slip correction factors for the respective diameters D_B and D_m. $C(D)$ can be approximated by the empirical relation (Willeke and Baron, 2001):

$$C(D) = 1 + \frac{2\lambda}{D}\left(1.142 + 0.558\,\exp\left(-0.999\frac{D}{2\lambda}\right)\right) \quad (30)$$

in which λ is the mean free path of the gas molecules (λ=68 nm in air at 298 K and atmospheric pressure).

In a calibration of the CCNC using particles generated by an aqueous solution of sodium chloride, the particle size selected by the DMA is the electrical mobility diameter (D=D_B). The mobility equivalent diameters D_B have to be transformed into mass equivalent diameters D_m via Eq. (29). Using Eq. (30), Eq. (29) has to be solved iteratively for D_m, setting χ=1.08 as a shape factor for cubic shaped particles. The so determined D_m are taken as the mass equivalent diameters of the dry salt particles (D_s) and used for all further calculations (such as determining D_{50} using Eq. (1), and calculating S_c as described in Sects. 3.1 to 3.5).

The nebulization of an ammonium sulfate solution is generally assumed to generate particles of near-spherical shape. Recent investigations indicate that shape corrections may also be required for ammonium sulfate particles in studies aimed at high accuracy (Eugene Mikhailov, personal communication). In the model calculations performed in this study, however, we assumed $D_B \approx D_m$ for ammonium sulfate and discuss the implications of possible deviations in Sect. 4.7.

4 Results

4.1 Effect of doubly charged particles on CCN efficiency spectra

Figure 3 shows exemplary CCN efficiency spectra and fit curves used to determine the dry particle diameter of 50% activation, D_{50}, which is the basis for calculating the

effective water vapor supersaturation in the CCN counter, S_{eff}. As outlined in Sect. 2.3, CCN efficiency spectra recorded by particle size selection with a differential mobility analyzer can be influenced by doubly charged particles (cf. Fig. 2a) which interfere with the determination of D_{50}.

The measured spectrum in Fig. 3a exhibits a high fraction of activated doubly charged particles (plateau level ~0.17). The fit with a single cumulative Gaussian distribution function (Eq. 1) strongly deviated from the measured data points and gave a D_{50} value ~2% smaller than the value obtained by fitting with two distribution functions. After correcting the measured spectrum with Eq. (2), the fit of Eq. (1) to the corrected spectrum gave the same D_{50} value as the fit of two distribution functions to the uncorrected spectrum, which can be regarded as the actual particle diameter of 50% activation. The ~2% increase of D_{50} led to a ~3% relative decrease of the effective supersaturation determined by Köhler model calculations. The measured spectrum in Fig. 3b exhibits a low fraction of activated doubly charged particles (plateau level ~0.06), and the fit with a single cumulative Gaussian distribution function (Eq. 1) agrees well with all data points at CCN/CN >0.1. Therefore, the D_{50} value obtained from this fit was only ~0.5% smaller than the values obtained after correcting the spectrum with Eq. (2), or fitting with two distribution functions, and the relative change of S_{eff} was only 0.7%.

In our study, the observed fraction of activated doubly charged particles was generally in the range of 0–0.25. In most cases the fraction was < 0.1 and a single cumulative Gaussian distribution (Eq. 1) fitted to the data points was used to determine D_{50} (relative deviations of D_{50} and $S_{eff} \leq 1\%$). For plateau levels >0.1, two cumulative Gaussian distributions were used.

4.2 Measurement precision within a calibration experiment

Figure 2a shows the CCN efficiency curves and Table 6 presents the measured and calculated values of an exemplary calibration experiment with ammonium sulfate particles. The experiment lasted for 26 h and was performed in the laboratory under

ACPD
7, 8193–8260, 2007

stable surrounding conditions at an ambient pressure of 1026±2 hPa and a sample temperature of, on average, 23.1±0.2°C. The temperature T_1, which was used for the Köhler calculations, was on average 25.3 ±0.2°C.

In this calibration experiment, the plateau level of activated doubly charged particles was <0.05 for all scans. The CCN efficiency spectrum was not corrected for doubly charged particles, because in the previous section it was shown that their effect is <1% on S_{eff} for such a small level. The fitting of a cumulative Gaussian distribution (Eq. 1) to the measured spectrum was used to determine D_{50}. The D_{50} values obtained from the fits were 178, 61, 45, 33, and 26 nm for the 5 different ΔT values (1.8, 5.1, 7.7, 11.7, and 15.6 K). The 95% confidence interval for D_{50} was, on average, less than 2 nm, which confirms the skill of the fit function used. The standard deviation of D_{50} at a given temperature difference was very small, when the measurements were performed at nearly constant surrounding conditions (constant ambient pressure and temperature) over many hours (15 repeats per ΔT; with a variation in ΔT of around ±0.03 K). It decreased with increasing supersaturation, ranging from 0.3–1.4% in diameter.

Using the D_{50} values obtained from the CCN efficiency spectra, critical supersaturations S_c were calculated as described in Sect. 3.4 using the VH4.1 model, and these were taken as the effective supersaturations in the CCNC, S_{eff}. The supersaturations corresponding to the 5 set ΔTs (as mentioned above) were 0.06, 0.32, 0.52, 0.84, and 1.22%. The relative uncertainty in the supersaturation due to the measurement uncertainty of D_{50} (i.e., standard deviation of D_{50}) was as much as 2.2% (relative). The uncertainty decreased with increasing supersaturation.

From each CCN efficiency spectrum, the derived S_{eff} was plotted versus the applied ΔT, and a linear calibration function was obtained by fitting (cf. Fig. 2b) as described in Sect. 2.3. For the experiment discussed here, we obtained $S_{\text{eff}}=0.0838\cdot\Delta T - 0.1097$ with $R^2=0.9974$. In spite of the high R^2 value, the deviations of measured data points from the fit line were substantial at small supersaturations. At $S_{\text{eff}}\approx 0.06\%$, the calibration line deviated by 38% (relative) from the experimentally determined supersaturation, indicating that in this range S_{eff} is not linearly dependent on ΔT. At

ACPD
7, 8193–8260, 2007

EGU

higher supersaturations (S_{eff}>0.1%), however, the calibration line agreed very well with the experimental data points (relative deviations ≤3%).

4.3 Variability within and between different measurement campaigns

We have operated our DMT-CCNC at a variety of locations and elevations. Calibration measurements were made during two one-month field campaigns in Guangzhou and Beijing, China, at our home laboratory in Mainz, Germany, at a laboratory in Leipzig, Germany, and at two mountain stations, Hohenpeissenberg, Germany, and Jungfraujoch, Switzerland (Figs. 4a–d). In the first campaign in Guangzhou (Fig. 4a), the CCNC was running with a flow rate of 0.5 L min^{-1} at close to standard atmospheric pressure, and T_1 varied between 25 and 30°C. A mean calibration line was calculated to provide an average S_{eff} to ΔT relationship over the whole field campaign. Here, the first calibration measurement was not taken into account, because it was measured at a T_1 that was much higher than during the rest of the campaign. It is evident that, in spite of the small variations in T_1 (25 to 26.7°C), the measured calibration lines differed significantly from the mean line, and exhibited maximum deviations in S_{eff} from the average supersaturation of 5–7% (relative).

The calibration lines from the second campaign in Beijing (Q=0.5 L min^{-1}, p≈1020 hPa; Fig. 4b), also scattered over time. Here, the maximum deviations in S_{eff} from the average supersaturation were also in the range of 5–7%, although the variations in T_1 were a little more (25.4 to 29°C).

Before and after each field campaign, we always calibrated the CCNC in our home laboratory (Mainz, p≈1020 hPa). In December 2005, we performed a calibration measurement using the same experimental setup over several days. The instrument was stopped in between measurement runs only to make small changes (change of dilution flow, liquid flow, etc.). The period was divided into five individual calibration experiments with the resulting calibration lines shown in Fig. 4c. The five calibration lines differed from an average curve by up to 2% (relative) in supersaturation.

In 2006, we made three more calibrations experiments (Fig. 4c) in our laboratory.

ACPD
7, 8193–8260, 2007

EGU

The time between each experiment was more than one month and the experimental setup was newly arranged every time. The three calibration lines obtained also scattered around a mean curve by up to 2–3% in supersaturation. From Fig. 4c, it can be seen that the slope of the mean calibration line was considerably smaller (10.4%) than it was for the measurements in December 2005. We assume that the performance of the CCNC changed during this time. Over the complete one-year period, the supersaturation calibrated against ΔT in our laboratory varied by up to ±6% from the average S_{eff}.

Figure 4d shows the calibration lines measured during field campaigns at mountain stations (Hohenpeissenberg, 900 m a.s.l.; Mt. Jungfraujoch, 3570 m a.s.l.) and in a laboratory near sea level (Leipzig). It illustrates that the supersaturation obtained at a given ΔT decreases significantly with pressure, which will be discussed in more detail in Sect. 4.5.

For the two field campaigns on Mt. Jungfraujoch we found a similar long-term trend as for the lab experiments. The calibration line in 2007 has a 16% lower slope than that in 2006, whereas the calibration lines within one campaign hardly differ from each other.

4.4 Application of the CCNC flow model

Four calibration experiments performed at different locations, altitudes and flow rates (cf. Table 5; MZ05, MZ10, JF05, JF08) were used to determine the thermal resistance (R_T) of our CCN instrument according to the procedure described in Sect. 2.4 and based on the model described by Lance et al. (2006). Figure 5 shows the calculated R_T as a function of ΔT. It can be seen that R_T varies with ΔT, and differs between the different calibration runs. The overall average R_T calculated for $\Delta T \geq 3$ K was $1.78\,\text{K}\,\text{W}^{-1}$, which was assumed to be the valid thermal resistance for our CCNC unit. The R_T values for $\Delta T < 3$ K were not included in the average, because the values were calculated for conditions under which S_{eff} might not depend linearly on ΔT, which makes the R_T values unreliable.

Using the average R_T, the calibration lines of the example conditions shown in Table 7 were modeled as described in Sect. 2.4 and compared with the experimentally determined curves (Fig. 6). Except for the calibration experiment MZ10, the modeled lines agree well with the experimentally determined curves – also for HP05, which had not been included in the determination of R_T. Only in the low supersaturation range (<0.1%) did the model deviate strongly from the measured S_{eff} by up to 28% (relative). At high S_{eff}, the relative deviations between model predictions and measurement values were on average +0.4% for MZ05, –3.5% for JF08, +2.3% for JF05, and +5.8% for HP05. Individual data points deviated by up to ~8%. For the MZ10 example, the modeled S_{eff} was on average 73% too high. This discrepancy might be due to instabilities during the calibration experiment, indicated by relatively large deviations of the measured data points from linearity.

As outlined in Sect. 2.4, the parameterizations of Lance et al. (2006) used to determine the thermal resistance of the CCNC were based on a van't Hoff factor model with i_s=3. Accordingly, the best agreement between flow model and experimental calibration results was achieved when using the VH4.3 Köhler model to calculate S_{eff} from D_{50}. Figure 6 also shows the measured calibration lines for which the S_{eff} was calculated using the VH4.1 Köhler model (the one that we used in general for our calculations). For the example cases MZ05, JF08, JF05, and HP05, the modeled S_{eff} was then on average 11%, 14%, 8%, and 6% lower than the experimental S_{eff}, respectively. The modeled calibration line for MZ10 agreed better with the experimental data calculated with the VH4.1 Köhler model than with the experimental data calculated with VH4.3, but especially the low S_{eff} were still up to ~60% too high.

4.5 Dependence of supersaturation on temperature, pressure, and flow rate

As shown in Sect. 4.3 (Fig. 4), the relation between S_{eff} and ΔT depends on T_1, p, and Q. Here we characterize and compare the dependencies observed in calibration experiments at different temperatures, flow rates, and pressures with the results of CCNC flow model calculations (cf. Sects. 2.4 and 4.4).

To investigate the dependence of S_{eff} on T_1, we used all calibration lines measured at a flow rate of 0.5 L min^{-1} and standard atmospheric pressure to calculate S_{eff} at ΔT=5 K, which corresponds to an inner-column temperature gradient of ~8 K m^{-1} (subtraction of $\Delta T_0 \approx 1$ K and divison of $\Delta T^* \approx 4$ K by the column length of 0.5 m; cf. Sect. 2.4). When plotted against T_1 (Fig. 7a), the experimentally determined S_{eff} values exhibit a near linear decreasing trend with an average slope of $\Delta S_{eff}/\Delta T_1$=–0.0057% K^{-1}. The observed dependence agrees fairly well with flow model calculations for the same conditions (Q=0.5 L min^{-1}, p=1020 hPa, and ΔT=5 K) yielding a slope of $\Delta S_{eff}/\Delta T_1$=–0.0049% K^{-1}. Both values are of similar magnitude but somewhat higher than the –0.0034% K^{-1} calculated by Roberts and Nenes (2005) for an inner-column temperature gradient of 8.3 K m^{-1}. Note, however, that the observed variability of S_{eff} at $T_1 \approx 299$ K was of similar magnitude as the observed and modeled differences between 296 K and 303 K.

Figure 7b illustrates the dependence of S_{eff} on pressure. All calibration lines presented in Fig. 4 were used to calculate the effective supersaturation at ΔT=5 K, and the obtained values were plotted against pressure. The observed near-linear increase of S_{eff} with p was 0.037% per 100 hPa at Q=0.5 L min^{-1}, which is of similar magnitude as the flow model result (0.027% per 100 hPa) and the value reported by Roberts and Nenes (2005) ($\Delta S_{eff}/\Delta p$=+0.03% per 100 hPa for 0.5 L min^{-1} and dT/dZ=8.3 K m^{-1}).

Figure 7c shows the dependence of S_{eff} on the flow rate of the CCNC. All calibration lines measured at ~1020 hPa and ~650 hPa were used to calculate S_{eff} at ΔT=5 K, and the obtained values were plotted against Q. The observed increase of S_{eff} with Q was 0.029% per 0.1 L min^{-1} at sea level, and 0.042% per 0.1 L min^{-1} at high altitude. The model slopes were $\Delta S_{eff}/\Delta Q$=+0.048% per 0.1 L min^{-1} at 1020 hPa and $\Delta S_{eff}/\Delta Q$=+0.030% per 0.1 L min^{-1} at 650 hPa, respectively. The corresponding value reported by Roberts and Nenes (2005) was somewhat higher: $\Delta S_{eff}/\Delta Q$=0.06 % per 0.1 L min^{-1} for 1000 hPa and dT/dZ=8.3 K m^{-1}.

Figure 8 illustrates the observed average relative change of supersaturation

($\Delta S_{eff}/S_{eff}$) caused by changes of column top temperature, pressure, and flow rate as a function of ΔT.

The relative decrease of S_{eff} with increasing T_1 was ~2% K^{-1} at high ΔT and decayed near-exponentially to ~0.5% K^{-1} at ΔT=2 K (Fig. 8a). The relative increase of S_{eff} with increasing p was ~1% per 10 hPa at high ΔT and grew near-exponentially to ~ 2.3% per 10 hPa at ΔT=2 K. At high ΔT the relative increase of S_{eff} with increasing Q was ~15% per 0.1 L min^{-1} for the measurements at p≈1020 hPa and ~25% per 0.1 L min^{-1} at p≈650 hPa. For the 650 hPa measurements, the deviation increased with decreasing ΔT to up to ~30% per 0.1 L min^{-1} at ΔT=2 K, but for the measurements at ≈1020 hPa it decreased to almost –30% per 0.1 L min^{-1} at ΔT=2 K. The latter is most likely due to instabilities in the calibration experiment performed at 1 L min^{-1} and p≈1020 hPa (MZ10, cf. Fig. 6).

4.6 Deviations between different Köhler model calculations

To characterize the uncertainties related to Köhler model calculations, critical supersaturations were calculated for ammonium sulfate and sodium chloride particles in the size range of 20–200 nm using different Köhler models (AP, OS, VH, and AA, cf. Sects. 3.2–3.5) with different parameterizations and approximations of aqueous solution properties. An overview of the tested models and parameterizations is given in Table 5 (T=298.15 K unless stated otherwise). The results are summarized in Tables 8 and 9, and Figs. 9 and 10.

To test the influence of different parameterizations of the solution density and surface tension on S_c, we calculated S_c for ammonium sulfate particles based on the AP1.1 model using alternative parameterizations for ρ_{sol} and σ_{sol}. Assuming volume additivity to calculate ρ_{sol} (AP1.2), instead of calculating it from the experimental parameterizations by Tang and Munkelwitz (1994) (AP1.1), led to a S_c that was less than 0.5% lower. Using the density of pure water to approximate ρ_{sol} (AP1.3) lowered the supersaturation by up to ~1%. The approximation of σ_{sol} as σ_w (AP1.4) reduced S_c

by up to 1.5% and setting σ_{sol}=0.072 N m^{-1} (AP1.5) caused a 2% lower S_c at most. For all these test cases, the deviation in S_c decreased with increasing particle diameter. For the largest diameters, the approximations of ρ_{sol} and σ_{sol} had no significant influence on S_c.

The same test cases, when applied to sodium chloride, brought smaller deviations in S_c than for ammonium sulfate, namely –0.1% for AP1.2, –0.4% for AP1.3, –0.6% for AP1.4, and –1% for AP1.5 at most.

To investigate the different water activity parameterization models and their impact on S_c, the model approaches of AP1.2, and AP2 were applied to both ammonium sulfate and sodium chloride particles. The parameterizations of ρ_{sol} and σ_{sol} were fixed in each case. For ammonium sulfate, the S_c calculated with a_w by Kreidenweis et al. (2005) (AP2) was up to 2.7% higher than the S_c calculated with a_w by Tang and Munkelwitz (1994) (AP1.2). The deviation in S_c decreased for smaller diameters down to a ∼1% lower S_c for 20 nm. For sodium chloride, S_c was ∼5% smaller for the AP2 model calculations than for AP1.2 over the whole diameter range.

The OS model was compared with the AP model and resulted, for ammonium sulfate, in a 7–15% lower S_c (for 20 and 200 nm, respectively) with the OS model than with AP1.1. For sodium chloride, the S_c was between 2.9 and 4.9% (for 200 and 20 nm, respectively) higher with the OS model. The VH1.1 model was compared with the AP1.1 model and resulted for ammonium sulfate in a 7.1 to 13.7% lower S_c (for 20–200 nm, respectively) with the VH1.1 model than with AP1.1.

The results of the different VH models were compared for ammonium sulfate particles. Here, ρ_{sol} and σ_{sol} were parameterized as dependent on temperature and composition in all cases. For the van't Hoff factor, the composition dependent parameterizations (Eqs. 26 and 27) were always used. Only the Köhler equation was changed resulting in the three test cases VH1.1, VH2.1, and VH3.1. The non-simplified VH model (VH1.1) resulted in a S_c between 1.85 and 0.05% for particle diameters between 20 and 200 nm. The simplification of $i_s \approx \nu_s \Phi_s$(VH2.1) led to a value of S_c which was up to 0.3% lower than calculated with the VH1.1 model. The further

ACPD
7, 8193–8260, 2007

EGU

assumption that the contribution of the solute to the total mass of the droplet is so low that it could be neglected (VH3.1) resulted in an up to 2% higher S_c than that calculated with VH1.1. The influence of approximating solution densities and surface tensions by those of pure water was practically the same for base cases VH1-VH3 as for AP1 (~1% for ρ_{sol}; ~2% for σ_{sol}).

The VH4.1 model assumed, furthermore, that ρ_{sol} can be approximated with ρ_w. The critical supersaturations which were obtained by the VH4.1 model had up to 0.6% higher values than those calculated with VH1.1. A further simplification of case VH4.1 was to assume a constant van't Hoff factor. Using i_s=2.2 (VH4.2) led to a higher S_c than with VH4.1. The deviation increased with particle diameter up to 10%. Using i_s=3 (VH4.3) led to a lower S_c than with VH4.1. The deviation decreased with particle diameter from 15.3% at 20 nm to 5.6% at 200 nm.

The analytical approximation model results (AA.1) were compared for ammonium sulfate particles with the AP1.1 results (±2.5% deviation in S_c), with the VH1.1 results (up to 19% higher S_c), and with the OS model results (up to 21% higher S_c). For sodium chloride the AA.1 model calculations were compared with the AP1.1, with OS, and with VH4.2. The AA.1 calculations resulted in a S_c which was 8–10%, 3–7%, and ~8% higher than the respective compared model results.

To examine how sensitive S_c is to variations in the temperature, we compared the VH4.1 model (with T=298.15 K) with VH4.4 (with T=303.15 K). Calculations with the VH4.4 model resulted in a ~4% lower S_c than with VH4.1. Further, we investigated how much the S_c of NaCl particles would be underestimated if no shape correction were applied to the particle diameter. Calculating S_c from the uncorrected D_s using the AP1.1 model resulted in a 5.8–7.4% lower S_c than was calculated from the corrected diameters.

4.7 CCN activation of ammonium sulfate and sodium chloride particles: consistencies and discrepancies between experimental results and thermodynamic parameterizations

For comparison of Köhler models and thermodynamic parameterizations of ammonium sulfate and sodium chloride, the CCNC was calibrated with both substances in several laboratory experiments immediately following each other under practically identical conditions: Q=(0.5±0.001) L min^{-1}, p=(999±6) hPa, T_1=(299.6±0.5) K. For the experiment with sodium chloride, the diameters selected by the DMA were corrected for cubic shape (cf. Sect. 3.6). D_{50} was obtained as described in Sect. 2.3, and S_{eff} was calculated using selected Köhler models. The different resulting calibration lines (S_{eff} vs. ΔT) are shown in Fig. 11.

Note: for calculating S_{eff} with the NaCl-AP2 model, a shape correction was not applied, because the water activity parameterization used in this model already included shape corrections for NaCl (Kreidenweis et al., 2005).

For ammonium sulfate, AP1.1 was chosen as one of the models with highest S_{eff} values, VH4.3 as the one with lowest S_{eff} values, and VH4.1 as the standard model of this study with intermediate S_{eff} values (Sect. 4.6). AP2 is not displayed in Fig. 11 because it can hardly be distinguished from AP1.1. At high S_{eff}, $(NH_4)_2SO_4$-AP2 was less than 1% higher than $(NH_4)_2SO_4$-AP1.1, at low S_{eff} $(NH_4)_2SO_4$-AP2 was 5 % higher. The agreement confirms the consistency of the underlying thermodynamic data sets for aqueous solutions of ammonium sulfate determined in EDB and HTDMA hygroscopic growth experiments. The $(NH_4)_2SO_4$-VH4.1 model based on concentration-dependent van't Hoff factors from bulk solution measurements was more than 8% lower than $(NH_4)_2SO_4$-AP1.1. The $(NH_4)_2SO_4$-VH4.3 model, assuming a constant van't Hoff factor of i_s=3, was 16–20% lower than $(NH_4)_2SO_4$-AP1.1.

For sodium chloride, OS was chosen as one of the models with highest S_{eff} values, AP2 as the one with lowest S_{eff} values, and AP1.1 with intermediate S_{eff} values. The NaCl-AP1.1 and NaCl-AP2 models did not agree as well as for ammonium sulfate.

ACPD
7, 8193–8260, 2007

EGU

NaCl-AP1.1 was 4–5% higher than NaCl-AP2 in the whole supersaturation range, indicating that the underlying thermodynamic data sets for aqueous solutions of NaCl determined in EDB experiments (AP1.1) and HTDMA experiments (AP2) are not fully consistent. The NaCl-OS model based on data from NaCl bulk solution measurements was 3–5% higher than NaCl-AP1.1 and 10% higher than NaCl-AP2.

Upon comparison of ammonium sulfate and sodium chloride, each of the two model types AP1.1 and AP2 yielded different calibration lines. The S_{eff} values obtained from the $(NH_4)_2SO_4$ calibration experiment were 3–8% higher for AP1.1 and 11–13% higher for AP2 than the S_{eff} values obtained from the NaCl calibration experiment. These deviations indicate that the applied thermodynamic parameterizations for ammonium sulfate are not fully consistent with those for sodium chloride, neither with regard to the underlying EDB data sets (AP1.1) nor with regard to the HTDMA data sets (AP2).

The S_{eff} values obtained from the $(NH_4)_2SO_4$ experiment using the VH4.1 model agreed fairly well with the supersaturations derived from the NaCl experiment using the AP1.1 and AP2 models (deviations $<\sim$3% at $S_{\mathrm{eff}}\geq$0.3%, and up to $\sim$7% at S_{eff}=0.15% for AP1.1, and deviations <3% for AP2).

The agreement indicates that the concentration-dependent van't Hoff factors of Low (1969) and Young and Warren (1992) for $(NH_4)_2SO_4$ are consistent with the activity parameterizations of both Tang (1996) and Kreidenweis et al. (2005) for NaCl. In any case, the calibration line obtained with the $(NH_4)_2SO_4$-VH4.1 model lies in the middle of both the $(NH_4)_2SO_4$ and the NaCl calibration lines displayed in Fig. 11. Therefore, the VH4.1 model indeed appears to be best-suited for CCNC calibration with ammonium sulfate, as long as the discrepancies between the different activity parameterizations from hygroscopic growth experiments (EDB: AP1; HTDMA: AP2; bulk solution: OS and VH1.1-VH4.1) have not been resolved.

As outlined in Sect. 3.6, recent investigations indicate that for ammonium sulfate particles shape corrections may also be required to achieve high accuracy (Eugene Mikhailov, personal communication).

Taking the shape irregularities into account, all ammonium sulfate calibration lines

ACPD
7, 8193–8260, 2007

EGU

would be lifted by a few percent depending on envelope shape and porosity of the particles, respectively (Mikhailov et al., 2004). In this case, $(NH_4)_2SO_4$-AP1.1 and $(NH_4)_2SO_4$-AP2 would significantly exceed NaCl-OS and deviate even more from NaCl-AP1.1 and NaCl-AP2. On the other hand, $(NH_4)_2SO_4$-VH4.1 would still agree well with NaCl-AP1.1.

5 Conclusions

Table 10 summarizes the CCNC calibration and measurement uncertainties determined in this study. Under stable operating conditions, the effective water vapor supersaturation in the DMT-CCNC can be adjusted with high precision. The relative standard deviations of repeated measurements in laboratory experiments were as low as ±1% for S_{eff}>0.1%, but increased up to ±7% during field measurements, which is mostly due to variations of the CCNC column top temperature with ambient temperature. The observed dependence of S_{eff} on temperature (T_1), pressure (p), and aerosol flow rate (Q) in the CCNC can be approximated by the following gradients: $(\Delta S_{eff}/S_{eff})/\Delta T_1 \approx -2\%\ K^{-1}$ at $p \approx 1020$ hPa and $Q=0.5$ L min^{-1}; $(\Delta S_{eff}/S_{eff})/\Delta p \approx +0.1\%$ hPa^{-1} at $Q=0.5$ L min^{-1} and $T_1 \approx 299$ K; and $(\Delta S_{eff}/S_{eff})/\Delta Q \approx +0.15\%$ (mL min^{-1})$^{-1}$ at $p \approx 1020$ hPa and $T_1 \approx 299$ K.

At high supersaturations (S_{eff}>0.1%), the experimental data points generally agreed well with a linear calibration function (S_{eff} vs. ΔT ; relative deviations ≤3%). At S_{eff}<0.1%, however, the calibration line deviated by up to ~40% from experimental data points, indicating that in this range S_{eff} does not linearly depend on ΔT and special care has to be taken to obtain reliable measurements. Besides careful calibration, it may be beneficial to operate the CCNC at particularly low flow rates (<0.5 L min^{-1}) to achieve high precision at low S_{eff}.

In the course of several field and laboratory measurement campaigns extending over a period of about one year, we found a systematic decrease of the slope of the calibration line by about 10–15% which could not be reversed by standard cleaning

procedures and may require a full refurbishing of the instrument to be reversed. In any case, we recommend careful and repeated calibration experiments during every field campaign to ensure reliable operation and to obtaine representative uncertainty estimates for the CCN measurement data.

Besides experimental variabilities, Table 10 also summarizes calibration and measurement uncertainties related to data analysis and Köhler model calculations. If the influence of doubly charged particles is not taken into account in the fitting of CCN efficiency spectra, the 50% activation diameter can be underestimated, and the effective supersaturation can be overestimated by up to ~3%.

In Köhler model calculations, the approximation of the density and surface tension of aqueous salt solutions by those of pure water can lead to relative underestimations of S_{eff} which are small (–1% and –2%, respectively), but not negligible with regard to measurement precision under stable operating conditions. Most importantly, however, the Köhler model results obtained with different parameterizations and approximations of the activity of water in aqueous solution deviate by up to 25% for $(NH_4)_2SO_4$ and 15% for NaCl, respectively. To ensure the comparability of results, we suggest that CCN studies should always report exactly which Köhler model equations and parameterizations of solution properties were used for instrument calibration.

After the subtraction of a constant temperature offset and the derivation of an instrument-specific thermal resistance parameter ($R_T \approx 1.8\,\mathrm{K\,W^{-1}}$), the experimental calibration results could be fairly well reproduced by the CCNC flow model of Lance et al. (2006). At $S_{\mathrm{eff}}>0.1\%$ the relative deviations between flow model and experimental results were generally less than 8%, when the same Köhler model approach was used. At $S_{\mathrm{eff}}\leq 0.1\%$, however, the deviations exceeded 20%, which can be attributed to non-idealities which also cause the near-constant temperature offset. Therefore, we suggest that the CCNC flow model can be used for extrapolating the results of experimental calibrations to different operating conditions, but should generally be complemented by calibration experiments performed under the relevant conditions – during field campaigns as well as in laboratory studies. Moreover, the Köhler modeling

ACPD
7, 8193–8260, 2007

EGU

approach used in the CCNC flow model (constant van't Hoff factor i_s=3) deviates substantially from the more realistic modeling approaches tested and compared in this study. It yields by far the lowest S_{eff} values.

Substantial differences between the CCNC calibration results obtained with $(NH_4)_2SO_4$ and NaCl aerosols under equal experimental conditions (relative deviations of S_{eff} up to ~10%) indicate inconsistencies between widely used activity parameterizations derived from electrodynamic balance (EDB) single particle experiments (Tang and Munkelwitz, 1994; Tang, 1996) and hygroscopicity tandem differential mobility analyzer (HTDMA) aerosol experiments (Kreidenweis et al., 2005).

Nevertheless, the concentration-dependent van't Hoff factors of Low (1969) and Young and Warren (1992) for $(NH_4)_2SO_4$ were found to be consistent with the activity parameterizations of both Tang (1996) and Kreidenweis et al. (2005) for NaCl. Moreover, the calibration line obtained with the $(NH_4)_2SO_4$-VH4.1 model generally applied for CCNC calibration with ammonium sulfate in this study lies in the middle of both the $(NH_4)_2SO_4$ and the NaCl calibration lines. Indeed, the VH4.1 model appears to be best-suited for CCNC calibration with ammonium sulfate, as long as the discrepancies between the different activity parameterizations from hygroscopic growth experiments (EDB: AP1; HTDMA: AP2; bulk solution: OS and VH1.1-VH4.1) have not been resolved. Our investigations indicate a real need for further evaluation and experimental confirmation of preferred data sets and parameterizations for the activity of water in dilute aqueous $(NH_4)_2SO_4$ and NaCl solutions.

ACPD
7, 8193–8260, 2007

Notation

Symbol	Unit	Quantity
A_Φ	$(\mathrm{kg\ mol^{-1}})^{1/2}$	Debye-Hückel coefficient
a_w		water activity
c_s	$\mathrm{mol\ L^{-1}}$	molarity of the solute
D	m	measured (mobility equivalent) diameter of the dry particle
D_{50}	m	fit parameter; particle diameter at which half of the particles are activated
D_B	m	mobility equivalent diameter
D_c	m	critical dry particle diameter
D_m	m	mass equivalent diameter
D_s	m	mass equivalent diameter of the dry solute particle
D_{wet}	m	droplet diameter
$D_{\mathrm{wet},c}$	m	critical droplet diameter
g_s		particle growth factor
I	$\mathrm{mol\ kg^{-1}}$	ionic strength
i_s		van't Hoff factor of the solute
m_s	kg	mass of the dry solute
M_s	$\mathrm{kg\ mol^{-1}}$	molar mass of the solute
M_w	$\mathrm{kg\ mol^{-1}}$	molar mass of water
n_s	mol	number of moles of the solute
n_w	mol	number of moles of the solvent
p	Pa	pressure
Q	$\mathrm{L\ min^{-1}}$	total flow rate of the CCNC
R	$\mathrm{J\ K^{-1}\ mol^{-1}}$	universal gas constant
RH	%	relative humidity
R_T	$\mathrm{K\ W^{-1}}$	thermal resistance of the CCNC

ACPD
7, 8193–8260, 2007

s		water vapor saturation ratio
s_c		critical water vapor saturation ratio
S	%	supersaturation
S_c	%	critical supersaturation
S_{eff}	%	effective supersaturation of the CCNC
t	°C	temperature
T	K	absolute temperature
T_1	K	CCNC column top temperature
T_3	K	CCNC column bottom temperature
x_s		mass fraction of the solute in the droplet
z_1, z_2		numbers of elementary charges carried by the ions 1 and 2
Φ_s		molal or practical osmotic coefficient of the solute in aqueous solution
μ_s	mol kg^{-1}	molality of the solute
ΔT	K	temperature difference at the outer wall of the CCNC column
ΔT^*	K	flow model temperature difference
ΔT_0	K	temperature difference offset
ΔT_{inner}	K	temperature difference inside the CCNC column
η		thermal efficiency of the CCNC
ν_1, ν_2		numbers of positive and negative ions produced upon dissociation per formula unit of the solute
ν_s		stoichiometric dissociation number of the solute
ρ_s	kg m^{-3}	density of the dry solute
ρ_{sol}	kg m^{-3}	density of the solution droplet
ρ_w	kg m^{-3}	density of water
σ_{sol}	J m^{-2}	surface tension of a solution droplet
σ_w	J m^{-2}	surface tension of pure water

ACPD
7, 8193–8260, 2007

EGU

Acknowledgements. This work was funded by the Max Planck Society (MPG). The authors gratefully acknowledge support by the organizers, teams, hosts, and funding organizations of the measurement campaigns during which the reported calibration experiments have been performed: Beijing and Guangzhou: CAREBEIJING 2006 and PRIDE-PRD 2006, PKU; Hohenpeißenberg: ANTISTORM, and DWD; Mt. Jungfraujoch: CLACE-5 and -6, HFSJG, and SFB-TROPEIS; Leipzig: LExNo, IfT, and ACCENT. Thanks to T. W. Andreae for help in manuscript preparation.

References

Andreae, M. O., Hegg, D., Feichter, J., Kloster, S., Levin, Z., Liousse, C., Radke, L., and Stier, P.: Sources and nature of atmospheric aerosols, in: Scientific assessment of the effects of aerosols on precipitation, edited by Z. Levin & W. Cotton, World Meteorological Organization, 2007.

Andreae, M. O., Jones, C. D., and Cox, P. M.: Strong present-day aerosol cooling implies a hot future: Nature, 435, 1187–1190, 2005.

Andreae, M. O., Rosenfeld, D., Artaxo, P., Costa, A. A., Frank, G. P., Longo, K. M., and Silva-Dias, M. A. F.: Smoking rain clouds over the Amazon: Science, 303, 1337–1342, 2004.

Bilde, M. and Svenningsson, B.: CCN activation of slightly soluble organics: the importance of small amounts of inorganic salt and particle phase, Tellus B, 56, 128–134, 2004.

Brechtel, F. J. and Kreidenweis, S. M.: Predicting Particle Critical Supersaturation from Hygroscopic Growth Measurements in the Humidified TDMA. Part I: Theory and Sensitivity Studies, J. Atmos. Sci., 57, 1854–1871, 2000.

Broekhuizen, K., Pradeep Kumar, P., and Abbatt, J. P. D.: Partially soluble organics as cloud condensation nuclei: Role of trace soluble and surface active species, Geophys. Res. Lett., 31, L01107, doi:10.1029/2003GL018203, 2004.

Charlson, R. J., Seinfeld, J. H., Nenes, A., Kulmala, M., Laaksonen, A., and Facchini, M. C.: Reshaping the theory of cloud formation, Science, 292, 2025–2026, 2001.

Chen, J.-P.: Theory of Deliquescence and Modified Köhler Curves: Journal of the Atmospheric Sciences, 51, 3505–3516, 1994.

Chuang, P. Y., Collins, D. R., Pawlowska, H., Snider, J. R., Jonsson, H. H., Brenguier, J. L.,

Flagan, R. C., and Seinfeld, J. H.: CCN measurements during ACE-2 and their relationship to cloud microphysical properties, Tellus B, 52, 843–867, 2000.
Delene, D. J. and Deshler, T.: Calibration of a photometric cloud condensation nucleus counter designed for deployment on a balloon package, J. Atmos. Oceanic Technol., 17, 459–467, 2000.
Delene, D. J. and Deshler, T.: Vertical profiles of cloud condensation nuclei above Wyoming, J. Geophys. Res., 106, 12 579–12 588, 2001.
Dusek, U., Frank, G. P., Hildebrandt, L., Curtius, J., Schneider, J., Walter, S., Chand, D., Drewnick, F., Hings, S., Jung, D., Borrmann, S., and Andreae, M. O.: Size Matters More Than Chemistry for Cloud-Nucleating Ability of Aerosol Particles, Science, 312, 1375–1378, 2006.
Ervens, B., Cubison, M., Andrews, E., Feingold, G., Ogren, J. A., Jimenez, J. L., DeCarlo, P., and Nenes, A.: Prediction of cloud condensation nucleus number concentration using measurements of aerosol size distributions and composition and light scattering enhancement due to humidity, J. Geophys. Res., 112, D10S32, doi:10.1029/2006JD007426, 2007.
Frank, G. P., Dusek, U., and Andreae, M. O.: Technical note: A method for measuring size-resolved CCN in the atmosphere, Atmos. Chem. Phys. Discuss., 6, 4879–4895, 2006a.
Frank, G. P., Dusek, U., and Andreae, M. O.: Technical note: Characterization of a static thermal-gradient CCN counter, Atmos. Chem. Phys. Discuss., 6, 2151–2174, 2006b.
Gerber, H. E., Hoppel, W. A., and Wojciechowski, T. A.: Experimental verification of the theoretical relationship between size and critical supersaturation of salt nuclei, J. Atmos. Sci., 34, 1836–1841, 1977.
Giebl, H., Berner, A., Reischl, G., Puxbaum, H., Kasper-Giebl, A., and Hitzenberger, R.: CCN activation of oxalic and malonic acid test aerosols with the University of Vienna cloud condensation nuclei counter, J. Aerosol Sci., 33, 1623–1634, 2002.
Gras, J. L.: CN, CCN and particle size in Southern Ocean air at Cape Grim, Atmos. Res., 35, 233–251, 1995.
Gysel, M., Weingartner, E., and Baltensperger, U.: Hygroscopicity of Aerosol Particles at Low Temperatures. 2. Theoretical and Experimental Hygroscopic Properties of Laboratory Generated Aerosols, Environ. Sci. Technol., 36, 63–68, 2002.
Hänel, G.: The properties of atmospheric aerosol particles as functions of the relative humidity at thermodynamic equilibrium with the surrounding moist air, Adv. Geophys., 19, 73–188,

1976.
Hudson, J. G.: An Instantaneous CCN Spectrometer, J. Atmos. Oceanic Technol., 6, 1055–1065, 1989.
Hudson, J. G.: Cloud Condensation Nuclei, J. Appl. Meteorol., 32, 596–607, 1993.
Hudson, J. G. and Xie, Y.: Vertical distributions of cloud condensation nuclei spectra over the summertime northeast Pacific and Atlantic Oceans, J. Geophys. Res., 104, 30 219–30 229, 1999.
Hudson, J. G. and Yum, S. S.: Cloud condensation nuclei spectra and polluted and clean clouds over the Indian Ocean, J. Geophys. Res., 107, 8022, doi:10.1029/2001JD000829, 2002.
IAPSAG: International aerosol precipitation science assessment group (IAPSAG): Aerosol pollution impact on precipitation: a scientific review, 2007.
IPCC: Climate Change 2007: The Physical Science Basis: Summary for Policymakers. Contribution of Working Group I to the Fourth Assessment Report of the Intergovernmental Panel on Climate Change, 2007.
Khain, A., Rosenfeld, D., and Pokrovsky, A.: Aerosol impact on the dynamics and microphysics of deep convective clouds, Q. J. R. Meteorol. Soc., 131, 2639–2663, 2005.
Koehler, K. A., Kreidenweis, S. M., DeMott, P. J., Prenni, A. J., Carrico, C. M., Ervens, B., and Feingold, G.: Water activity and activation diameters from hygroscopicity data–Part II: Application to organic species, Atmos. Chem. Phys., 6, 795–809, 2006, http://www.atmos-chem-phys.net/6/795/2006/.
Köhler, H.: The nucleus in and the growth of hygroscopic droplets: Trans. Faraday Soc., 32, 1152–1161, 1936.
Krämer, L., Pöschl, U., and Niessner, R.: Microstructural rearrangement of sodium chloride condensation aerosol particles on interaction with water vapor, J. Aerosol Sci., 31, 673–685, 2000.
Kreidenweis, S. M., Koehler, K., DeMott, P. J., Prenni, A. J., Carrico, C., and Ervens, B.: Water activity and activation diameters from hygroscopicity data–Part I: Theory and application to inorganic salts, Atmos. Chem. Phys., 5, 1357–1370, 2005, http://www.atmos-chem-phys.net/5/1357/2005/.
Lance, S., Medina, J., Smith, J. N., and Nenes, A.: Mapping the Operation of the DMT Continuous Flow CCN Counter, Aerosol Sci. Technol., 40, 242–254, 2006.
Lohmann, U. and Feichter, J.: Global indirect aerosol effects: a review: Atmos. Chem. Phys., 5, 715–737, 2005,

http://www.atmos-chem-phys.net/5/715/2005/.
Low, R. D. H.: A theoretical study of nineteen condensation nuclei, Journal de Recherches Atmospheriques, 4, 65–78, 1969.
McDonald, J. E.: Erroneous cloud-physics applications of Raoult Law., J. Meteorol., 10, 68–78, 1953.
McFiggans, G., Artaxo, P., Baltensperger, U., Coe, H., Facchini, M. C., Feingold, G., Fuzzi, S., Gysel, M., Laaksonen, A., Lohmann, U., Mentel, T. F., Murphy, D. M., O'Dowd, C. D., Snider, J. R., and Weingartner, E., The effect of physical and chemical aerosol properties on warm cloud droplet activation, Atmos. Chem. Phys., 6, 2593–2649, 2006, http://www.atmos-chem-phys.net/6/2593/2006/.
Mikhailov, E., Vlasenko, S., Niessner, R., and Pöschl, U.: Interaction of aerosol particles composed of protein and salts with water vapor: hygroscopic growth and microstructural rearrangement, Atmos. Chem. Phys., 4, 323–350, 2004, http://www.atmos-chem-phys.net/4/323/2004/.
Mokbel, I., Ye, S., Jose, J., and Xans, P.: Study of non ideality of various aqueous sodium chloride solutions by vapor pressures measurements and correlation of experimental results by Pitzer's method, J. Chim. Phys., 94, 122–137, 1997.
Pitzer, K. S. and Mayorga, G.: Thermodynamics of electrolytes. II. Activity and osmotic coefficients for strong electrolytes with one or both ions univalent, J. Phys. Chem., 77, 2300–2308, 1973.
Pradeep Kumar, P., Broekhuizen, K., and Abbatt, J. P. D.: Organic acids as cloud condensation nuclei: Laboratory studies of highly soluble and insoluble species, Atmos. Chem. Phys., 3, 509–520, 2003, http://www.atmos-chem-phys.net/3/509/2003/.
Pruppacher, H. R. and Klett, J. D: Microphysics of clouds and precipitation. Dordrecht: Kluwer Academic Publishers, 2007.
Raymond, T. M. and Pandis, S. N.: Formation of cloud droplets by multicomponent organic particles, J. Geophys. Res., 108, 4469, doi:10.1029/2003JD003503, 2003.
Reade, L., Jennings, S. G., and McSweney, G.: Cloud condensation nuclei measurements at Mace Head, Ireland, over the period 1994–2002, Atmos. Res., 82, 610–621, 2006.
Roberts, G., Mauger, G., Hadley, O., and Ramanathan, V.: North American and Asian aerosols over the eastern Pacific Ocean and their role in regulating cloud condensation nuclei, J. Geophys. Res., 111, D13205, doi:10.1029/2005JD006661, 2006.

Roberts, G. C. and Nenes, A.: A Continuous-Flow Streamwise Thermal-Gradient CCN Chamber for Atmospheric Measurements, Aerosol Sci. Technol., 39, 206-221, 2005.
Robinson, R. A. and Stokes, R. H.: Electrolyte Solutions, (revised), London: Butterworth, 1959.
Rosenfeld, D. and Givati, A.: Evidence of orographic precipitation suppression by air pollution-induced aerosols in the western United States, J. Appl. Meteorol. Climatol., 45, 893–911, 2006.
Scheibel, H. G. and Porstendörfer, J.: Generation of monodisperse Ag-and NaCl-aerosols with particle diameters between 2 and 300 nm, J. Aerosol Sci., 14, 113–126, 1983.
Segal, Y. and Khain, A.: Dependence of droplet concentration on aerosol conditions in different cloud types: Application to droplet concentration parameterization of aerosol conditions, J. Geophys. Res., 111, D15204, doi:10.1029/2005JD006561, 2006.
Segal, Y., Khain, A., Pinsky, M., and Sterkin, A.: Sensitivity of raindrop formation in ascending cloud parcels to cloud condensation nuclei and thermodynamic conditions, Q. J. R. Meteorol. Soc., 130, 561–581, 2004.
Seinfeld, J. H. and Pandis, S. N.: Atmospheric Chemistry and Physics: From Air Pollution to Climate Change. New York: John Wiley & Sons, Inc., 1998.
Snider, J. R., Guibert, S., Brenguier, J.-L., and Putaud, J.-P.: Aerosol activation in marine stratocumulus clouds: 2. Köhler and parcel theory closure studies, J. Geophys. Res., 108, 8629, doi:10.1029/2002JD002692, 2003.
Snider, J. R., Petters, M. D., Wechsler, P., and Liu, P. S. K.: Supersaturation in the Wyoming CCN Instrument, J. Atmos. Oceanic Technol., 23, 1323–1339, 2006.
Tang, I. N.: Chemical and size effects of hygroscopic aerosols on light scattering coefficients, J. Geophys. Res., 101, 19 245–19 250, 1996.
Tang, I. N. and Munkelwitz, H. R.: Water activities, densities, and refractive indices of aqueous sulfates and sodium nitrate droplets of atmospheric importance, J. Geophys. Res., 99, 18 801–18 808, 1994.
Weast, R. C. and Astle, M. J.: CRC Handbook of Chemistry and Physics, 63rd. Florida: CRC Press Inc., 1982.
Wex, H., Kiselev, A., Stratmann, F., Zoboki, J., and Brechtel, F.: Measured and modeled equilibrium sizes of NaCl and (NH4)2SO4 particles at relative humidities up to 99.1%, J. Geophys. Res., 110, D21212, doi:10.1029/2004JD005507, 2005.
Wiedensohler, A.: An approximation of the bipolar charge distribution for particles in the submicron size range, J. Aerosol Sci., 19, 387–389, 1988.

Willeke, K. and Baron, P. A.: Aerosol Measurement: Principles, Techniques, and Applications. (2nd ed.). New York: John Wiley & Sons, Inc., 2001.
Young, K. C. and Warren, A. J.: A reexamination of the derivation of the equilibrium supersaturation curve for soluble particles, J. Atmos. Sci., 49, 1138–1143, 1992.

ACPD
7, 8193–8260, 2007

Table 1. Density and molar mass for NaCl and $(NH_4)_2SO_4$.

	NaCl	$(NH_4)_2SO_4$
density [kg m^{-1}]	2165	1770
molar mass [kg mol^{-1}]	58.44×10^{-3}	132.14×10^{-3}

ACPD
7, 8193–8260, 2007

EGU

Table 2. Polynomial coefficients used to calculate the water activity with Eq. (9) or (10). The coefficients a_1, a_2, a_3, and a_4 for $(NH_4)2SO_4$ and NaCl at 298 K are given in Tang and Munkelwitz (1994) and in Tang (1996), respectively. The coefficients k_a, k_b, and k_c are the Kelvin corrected values for $(NH_4)_2SO_4$ and the Kelvin and shape corrected values for NaCl, taken from Kreidenweis et al. (2005).

water activity parameters	$(NH_4)_2SO_4$	NaCl
a_1 [kg mol^{-1}]	-2.715×10^{-3}	-6.366×10^{-3}
a_2 [kg^2 mol^{-2}]	3.113×10^{-5}	8.624×10^{-5}
a_3 [kg^3 mol^{-3}]	-2.336×10^{-6}	-1.158×10^{-5}
a_4 [kg^4 mol^{-4}]	1.412×10^{-8}	1.518×10^{-7}
k_a	2.42848	5.78874
k_b	–3.85261	–8.38172
k_c	1.88159	3.9265

Table 3. Polynomial coefficients used to calculate the density of a solution droplet using Eq. (11). The coefficients d_1, d_2, d_3, and d_4 for $(NH_4)_2SO_4$ and NaCl at 298 K are given in Tang and Munkelwitz (1994) and in Tang (1996), respectively.

density parameters	$(NH_4)_2SO_4$	NaCl
d_1 [kg mol^{-1}]	5.92×10^{-3}	7.41×10^{-3}
d_2 [kg^2 mol^{-2}]	-5.036×10^{-6}	-3.741×10^{-5}
d_3 [kg^3 mol^{-3}]	1.024×10^{-8}	2.252×10^{-6}
d_4 [kg^4 mol^{-4}]	–	-2.06×10^{-8}

Table 4. Ion-interaction coefficients used to calculate the practical osmotic coefficients of ammonium sulfate and sodium chloride in aqueous solution at 298.15 K.

Salt	$(NH_4)_2SO_4$	NaCl	NaCl
Reference	Pitzer and Mayorga (1973)		Mokbel et al. (1997)
β_0 [kg mol^{-1}]	0.0409	0.0765	0.1018
β_1 [kg mol^{-1}]	0.6585	0.2664	0.2770
C_Φ [kg^2 mol^{-2}]	–0.0012	0.00127	0.00119

ACPD
7, 8193–8260, 2007

Table 5. Overview of the Köhler models described in Sect. 3 and compared in Sects. 4.6 and 4.7. This table lists the substances to which the model was applied (AS=ammonium sulfate; SC=sodium chloride), the Köhler equation used as well as the parameterizations for the solution density, the surface tension of the solution, the water activity, and the van't Hoff factor for all base cases and test cases. (* was tested at 303.15 K.).

model	substances	Köhler equation	density, ρ_{sol}	surface tension, σ_{sol}	water activity, a_w	van't Hoff factor, i_s
AP1.1	AS, SC	Eq. (16)	Eq. (11)	Eq. (14)	Eq. (9)	–
AP1.2	AS, SC	Eq. (16)	Eq. (12)	Eq. (14)	Eq. (9)	–
AP1.3	AS, SC	Eq. (16)	$\rho_{sol}=\rho_w$	Eq. (14)	Eq. (9)	–
AP1.4	AS, SC	Eq. (16)	Eq. (11)	$\sigma_{sol}=\sigma_w$	Eq. (9)	–
AP1.5	AS	Eq. (16)	Eq. (11)	$\sigma_{sol}=0.072\,\mathrm{Nm}^{-1}$	Eq. (9)	–
AP2	AS, SC	Eq. (16)	Eq. (12)	Eq. (14)	Eq. (10)	–
OS	AS, SC	Eq. (16)	Eq. (11)	Eq. (14)	Eq. (17)	–
VH1.1	AS	Eq. (16)	Eq. (11)	Eq. (14)	Eq. (19)	Eqs. (26), (27)
VH1.2	AS	Eq. (16)	Eq. (12)	Eq. (14)	Eq. (19)	Eqs. (26), (27)
VH1.3	AS	Eq. (16)	$\rho_{sol}=\rho_w$	Eq. (14)	Eq. (19)	Eqs. (26), (27)
VH1.4	AS	Eq. (16)	Eq. (11)	$\sigma_{sol}=\sigma_w$	Eq. (19)	Eqs. (26), (27)
VH1.5	AS	Eq. (16)	$\rho_{sol}=\rho_w$	$\sigma_{sol}=\sigma_w$	Eq. (19)	Eqs. (26), (27)
VH2.1	AS	Eq. (21)	Eq. (11)	Eq. (14)	–	Eqs. (26), (27)
VH2.2	AS	Eq. (21)	Eq. (12)	Eq. (14)	–	Eqs. (26), (27)
VH3.1	AS	Eq. (22)	Eq. (11)	Eq. (14)	–	Eqs. (26), (27)
VH3.2	AS	Eq. (22)	$\rho_{sol}=\rho_w$	Eq. (14)	–	Eqs. (26), (27)
VH3.3	AS	Eq. (22)	Eq. (11)	$\sigma_{sol}=\sigma_w$	–	Eqs. (26), (27)
VH4.1	AS	Eq. (23)	$\rho_{sol}=\rho_w$	–	–	Eqs. (26), (27)
VH4.2	AS, SC	Eq. (23)	$\rho_{sol}=\rho_w$	–	–	AS: i_s=2.2 SC: i_s=2
VH4.3	AS	Eq. (23)	$\rho_{sol}=\rho_w$	–	–	i_s=3
VH4.4*	AS	Eq. (23)	$\rho_{sol}=\rho_w$	–	–	Eqs. (26), (27)
AA.1	AS, SC	Eq. (28)	–	–	–	AS: i_s=2.2 SC: i_s=2
AA.2	AS	Eq. (28)	–	–	–	AS: i_s=3

ACPD
7, 8193–8260, 2007

EGU

Table 6. Measured and calculated averages and standard deviations for the experiment shown in Fig. 2.

number of scans	mean ΔT	stdev ΔT	mean D_{50}	relative stdev D_{50}	mean confidence interval for D_{50}	mean S_{eff}	relative stdev of S_{eff}	S_{eff} from calibration line fit	relative deviation of S_{eff} from fit
	[K]	[K]	[nm]	[%]	[nm]	[%]	[%]	[%]	[%]
15	1.84	0.02	178.3	1.4	1.7	0.062	2.2	0.044	38.5
15	5.10	0.03	61.3	0.9	0.6	0.318	1.3	0.317	0.2
15	7.71	0.03	44.7	0.6	0.3	0.519	0.9	0.536	3.2
15	11.66	0.02	32.8	0.6	0.2	0.840	1.0	0.867	3.1
15	15.59	0.02	25.8	0.3	0.6	1.223	0.5	1.197	2.2

ACPD
7, 8193–8260, 2007

EGU

Table 7. Calibration experiments used to model the supersaturation in the CCNC. The slope and intercept are given as the fit parameters of the calibration line using Köhler model VH4.3 to calculate S_{eff}.

name	date	location	p [hPa]	Q [L min^{-1}]	T_1 [°C]	slope (VH4.3)	intercept (VH4.3)
MZ05	19.12.2005	Mainz, lab	1023	0.5	25.7	0.0688	–0.07
MZ10	23.12.2005	Mainz, lab	1021	1.0	25.2	0.1384	–0.2928
JF08	08.02.2007	Jungfraujoch, field	650	0.8	26.1	0.0695	–0.0868
JF05	10.02.2007	Jungfraujoch, field	650	0.5	28.4	0.0432	–0.0622
HP05	11.01.2006	Hohenpeissenberg, field	902	0.5	25.1	0.0557	–0.0431

Table 8. Results for the critical supersaturations S_c in % calculated for ammonium sulfate particles with mobility equivalent dry diameters (D, equal to mass equivalent diameters D_s) in the range of 20–200 nm using different Köhler model approaches. Model VH4.1 (indicated in bold characters) was generally applied for CCNC calibration in this study unless mentioned otherwise.

D [nm]	20	30	40	50	60	70	80	90	100	110
AP1.1	1.9871	1.0585	0.6811	0.4849	0.3678	0.2913	0.2381	0.1993	0.1701	0.1473
AP1.2	1.9809	1.0568	0.6804	0.4846	0.3676	0.2912	0.238	0.1993	0.17	0.1473
AP1.3	1.9624	1.0518	0.6784	0.4836	0.367	0.2908	0.2378	0.1991	0.1699	0.1472
AP1.4	1.9588	1.0508	0.678	0.4834	0.3669	0.2907	0.2377	0.1991	0.1699	0.1472
AP1.5	1.9503	1.0463	0.6751	0.4813	0.3654	0.2895	0.2367	0.1982	0.1692	0.1466
AP2	1.9686	1.0653	0.6902	0.4932	0.3749	0.2973	0.2433	0.2038	0.174	0.1507
OS	1.8443	0.9683	0.6156	0.434	0.3265	0.2569	0.2088	0.1739	0.1478	0.1276
VH1.1	1.8455	0.9726	0.6201	0.4381	0.3302	0.2601	0.2116	0.1764	0.15	0.1295
VH1.2	1.8405	0.9713	0.6196	0.4379	0.33	0.26	0.2115	0.1764	0.15	0.1295
VH1.3	1.8257	0.9674	0.6181	0.4371	0.3296	0.2597	0.2114	0.1763	0.1499	0.1294
VH1.4	1.8228	0.9667	0.6178	0.437	0.3295	0.2597	0.2113	0.1763	0.1499	0.1294
VH1.5	1.8049	0.9617	0.6158	0.436	0.329	0.2594	0.2111	0.1761	0.1498	0.1293
VH2.1	1.8399	0.9711	0.6195	0.4378	0.33	0.26	0.2115	0.1764	0.15	0.1295
VH2.2	1.835	0.9698	0.619	0.4376	0.3299	0.2599	0.2115	0.1763	0.1499	0.1295
VH3.1	1.8816	0.9812	0.6233	0.4396	0.331	0.2606	0.2119	0.1767	0.1501	0.1296
VH3.2	1.8583	0.9756	0.6212	0.4386	0.3304	0.2602	0.2117	0.1765	0.15	0.1296
VH3.3	1.8549	0.9747	0.6209	0.4385	0.3304	0.2602	0.2117	0.1765	0.15	0.1295
VH4.1	**1.8342**	**0.9695**	**0.6188**	**0.4375**	**0.3298**	**0.2599**	**0.2114**	**0.1763**	**0.1499**	**0.1295**
VH4.2	1.8173	0.9852	0.6388	0.4567	0.3472	0.2754	0.2254	0.1888	0.1612	0.1397
VH4.3	1.5542	0.843	0.5468	0.3909	0.2973	0.2358	0.193	0.1617	0.138	0.1196
VH4.4	1.759	0.9301	0.5938	0.4199	0.3166	0.2494	0.203	0.1693	0.1439	0.1243
SS.1	1.9613	1.0629	0.6891	0.4926	0.3745	0.2971	0.2431	0.2037	0.1739	0.1507
SS.2	1.7801	0.9658	0.6267	0.4484	0.3412	0.271	0.2219	0.1861	0.159	0.138

Table 8. Continued.

D [nm]	120	130	140	150	160	170	180	190	200
AP1.1	0.1292	0.1146	0.1025	0.0924	0.0838	0.0765	0.0702	0.0648	0.0599
AP1.2	0.1292	0.1145	0.1025	0.0924	0.0838	0.0765	0.0702	0.0648	0.0599
AP1.3	0.1291	0.1145	0.1024	0.0923	0.0838	0.0765	0.0702	0.0647	0.0599
AP1.4	0.1291	0.1145	0.1024	0.0923	0.0838	0.0765	0.0702	0.0647	0.0599
AP1.5	0.1286	0.114	0.102	0.0919	0.0834	0.0762	0.0699	0.0645	0.0597
AP2	0.1322	0.1173	0.105	0.0947	0.0859	0.0784	0.0718	0.0664	0.0615
OS	0.1115	0.0986	0.088	0.0791	0.0717	0.0653	0.0598	0.0551	0.0509
VH1.1	0.1133	0.1002	0.0894	0.0804	0.0728	0.0664	0.0608	0.056	0.0517
VH1.2	0.1133	0.1002	0.0894	0.0804	0.0728	0.0664	0.0608	0.056	0.0517
VH1.3	0.1132	0.1001	0.0894	0.0804	0.0728	0.0663	0.0608	0.056	0.0517
VH1.4	0.1132	0.1001	0.0894	0.0804	0.0728	0.0663	0.0608	0.056	0.0517
VH1.5	0.1132	0.1001	0.0893	0.0804	0.0728	0.0663	0.0608	0.0559	0.0517
VH2.1	0.1133	0.1002	0.0894	0.0804	0.0728	0.0664	0.0608	0.056	0.0517
VH2.2	0.1133	0.1002	0.0894	0.0804	0.0728	0.0664	0.0608	0.056	0.0517
VH3.1	0.1134	0.1002	0.0895	0.0805	0.0729	0.0664	0.0608	0.056	0.0518
VH3.2	0.1133	0.1002	0.0894	0.0804	0.0728	0.0664	0.0608	0.056	0.0517
VH3.3	0.1133	0.1002	0.0894	0.0804	0.0728	0.0664	0.0608	0.056	0.0517
VH4.1	**0.1133**	**0.1001**	**0.0894**	**0.0804**	**0.0728**	**0.0664**	**0.0608**	**0.056**	**0.0517**
VH4.2	0.1226	0.1087	0.0973	0.0877	0.0796	0.0727	0.0667	0.0615	0.057
VH4.3	0.105	0.0931	0.0833	0.0751	0.0682	0.0623	0.0571	0.0527	0.0488
VH4.4	0.1087	0.0962	0.0858	0.0772	0.0699	0.0637	0.0584	0.0537	0.0497
SS.1	0.1322	0.1173	0.1049	0.0946	0.0859	0.0784	0.072	0.0664	0.0614
SS.2	0.1212	0.1076	0.0964	0.087	0.079	0.0722	0.0663	0.0612	0.0567

Table 9. Results for the critical supersaturations S_c in % calculated for sodium chloride particles with mobility equivalent dry diameters (D) in the range of 20–200 nm using different Köhler model approaches. The values of D correspond to the given mass equivalent diameters D_s.

D [nm]	20	30	40	50	60	70	80	90	100	110
D_s [nm]	19.2	28.8	38.4	48.0	57.6	67.1	76.7	86.2	95.7	105.2
AP1.1	1.209	0.6528	0.4228	0.3022	0.2298	0.1824	0.1493	0.1252	0.107	0.0928
AP1.2	1.2077	0.6524	0.4226	0.3021	0.2298	0.1824	0.1493	0.1252	0.107	0.0928
AP1.3	1.2045	0.6515	0.4222	0.3019	0.2296	0.1823	0.1493	0.1252	0.107	0.0928
AP1.4	1.202	0.6508	0.4219	0.3018	0.2296	0.1822	0.1492	0.1251	0.1069	0.0928
AP1.5	1.1969	0.6481	0.4202	0.3005	0.2286	0.1815	0.1486	0.1246	0.1065	0.0924
AP2	1.1485	0.6226	0.4036	0.2885	0.2194	0.174	0.1424	0.1193	0.1019	0.0883
OS	1.2679	0.6841	0.4421	0.3153	0.2393	0.1896	0.155	0.1298	0.1108	0.096
VH4.2	1.2121	0.6585	0.4275	0.306	0.2329	0.1849	0.1515	0.1271	0.1086	0.0942
SS.1	1.3079	0.7103	0.4612	0.33	0.2512	0.1995	0.1634	0.137	0.1171	0.1016

D [nm]	120	130	140	150	160	170	180	190	200
D_s [nm]	114.7	124.2	133.6	143.1	152.5	162.0	171.4	180.8	190.2
AP1.1	0.0815	0.0723	0.0648	0.0585	0.0531	0.0485	0.0446	0.0411	0.0381
AP1.2	0.0815	0.0723	0.0648	0.0585	0.0531	0.0485	0.0446	0.0411	0.0381
AP1.3	0.0815	0.0723	0.0648	0.0585	0.0531	0.0485	0.0446	0.0411	0.0381
AP1.4	0.0815	0.0723	0.0648	0.0584	0.0531	0.0485	0.0446	0.0411	0.0381
AP1.5	0.0811	0.072	0.0645	0.0582	0.0529	0.0483	0.0444	0.0409	0.038
AP2	0.0774	0.0687	0.0615	0.0554	0.0503	0.0459	0.0422	0.0388	0.036
OS	0.0842	0.0747	0.0669	0.0603	0.0547	0.05	0.0459	0.0424	0.0392
VH4.2	0.0827	0.0735	0.0658	0.0594	0.0539	0.0493	0.0453	0.0418	0.0387

ACPD
7, 8193–8260, 2007

EGU

Table 10. Overview of calibration and measurement uncertainties affecting the effective supersaturation in the CCNC (for S_{eff}>0.1%): statistical uncertainties are characterized by observed relative standard deviations (preceded by "±"); systematic uncertainties are characterized by observed/calculated maximum relative deviations (preceded by a sign indicating the direction of bias, if known).

Source of uncertainty	Characteristic relative deviation of S_{eff} (%)
Measurement precision in single experiment (hours)	±1
Variability of conditions in single field campaign (weeks)	±7
Deviations between different campaigns (months)	–10 to –16
Fitting of CCN efficiency spectra (double charging)	+4
Köhler model variants (solution density)	–1
Köhler model variants (surface tension)	–2
Köhler model variants (water activity, $(NH_4)_2SO_4$)	25
Köhler model variants (water activity, NaCl)	15
Köhler model variants (shape correction, NaCl)	–6
CCNC flow model extrapolations (T_1, p)	8

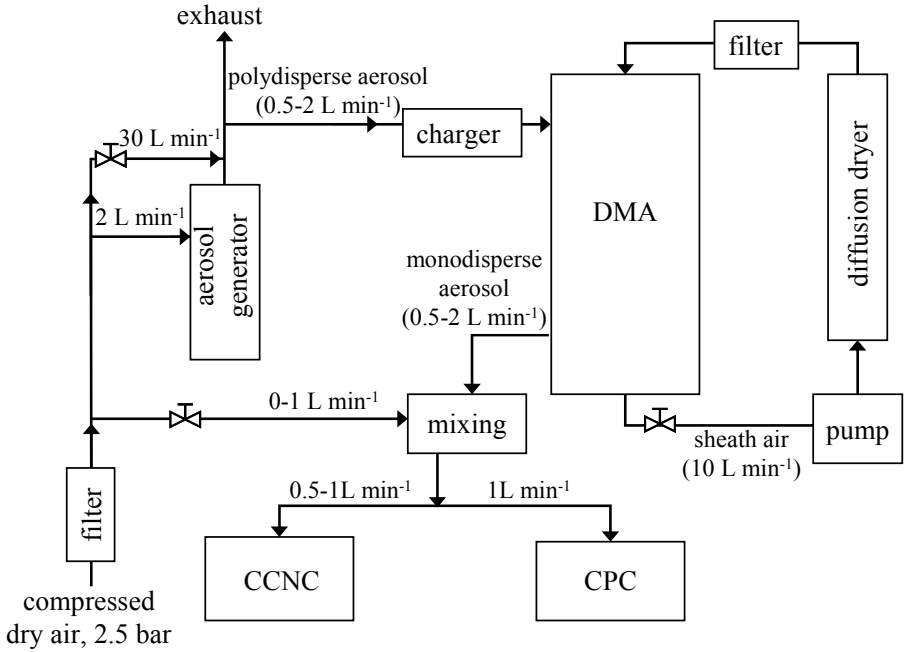

Fig. 1. Experimental setup: DMA – differential mobility analyzer, CCNC – cloud condensation nuclei counter, CPC – condensation particle counter.

ACPD
7, 8193–8260, 2007

EGU

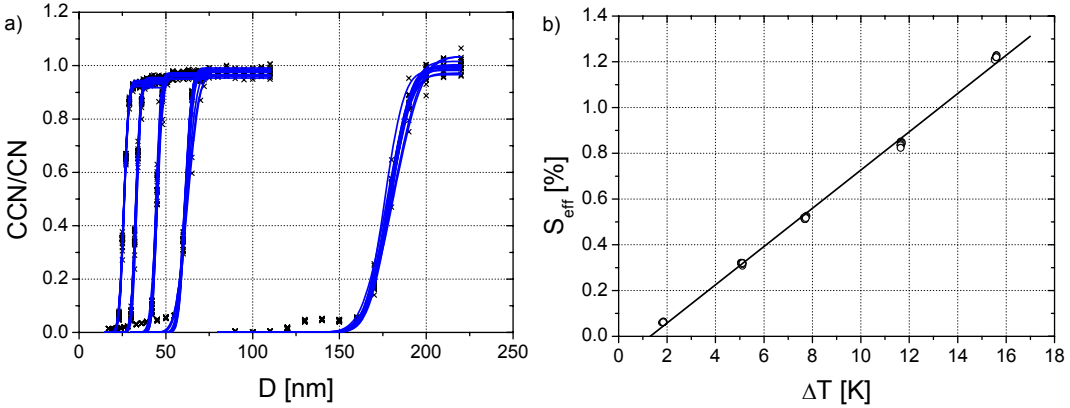

Fig. 2. Exemplary results of a laboratory calibration experiment with ammonium sulfate aerosol (Mainz, 21 December 2005, Q=0.5 L min^{-1}, p=1026 hPa, T_1=25.3°C): CCN efficiency spectra measured at 5 different ΔT values **(a)** and the corresponding calibration line **(b)**. The symbols are measurement data points and the solid lines are the cumulative Gaussian distribution (a) and linear fit (b) curves.

ACPD
7, 8193–8260, 2007

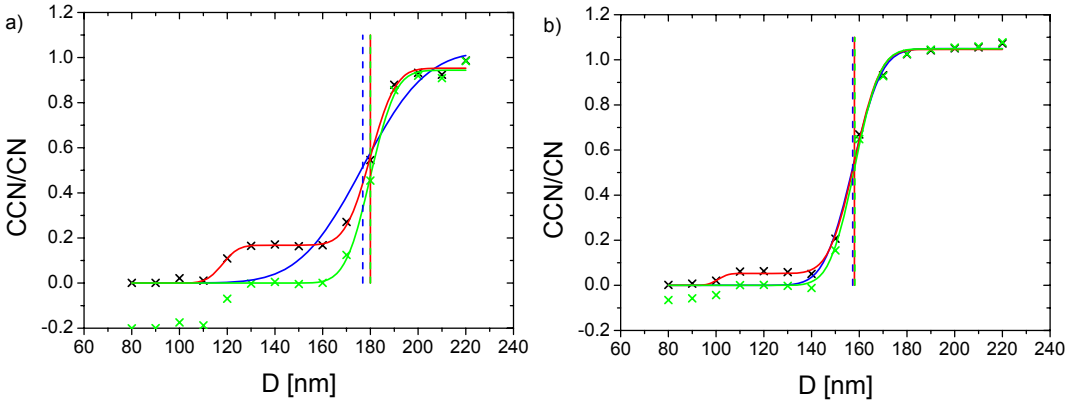

Fig. 3. Alternative fitting methods and diameters at which 50% of the monodisperse particles are activated (D_{50}) for exemplary CCN efficiency spectra with **(a)** high and **(b)** low fractions of doubly charged particles. The black crosses are measured data points. The green crosses are data points obtained by correction with Eq. (2). The blue line is the fit of a cumulative Gaussian distribution function (Eq. 1) to the measured spectrum and the green line is the fit of Eq. (1) to the corrected spectrum. The red line is the fit of two distribution functions to the measured spectrum. The vertical dashed lines are the D_{50} values obtained from the fit curves with the same color.

ACPD
7, 8193–8260, 2007

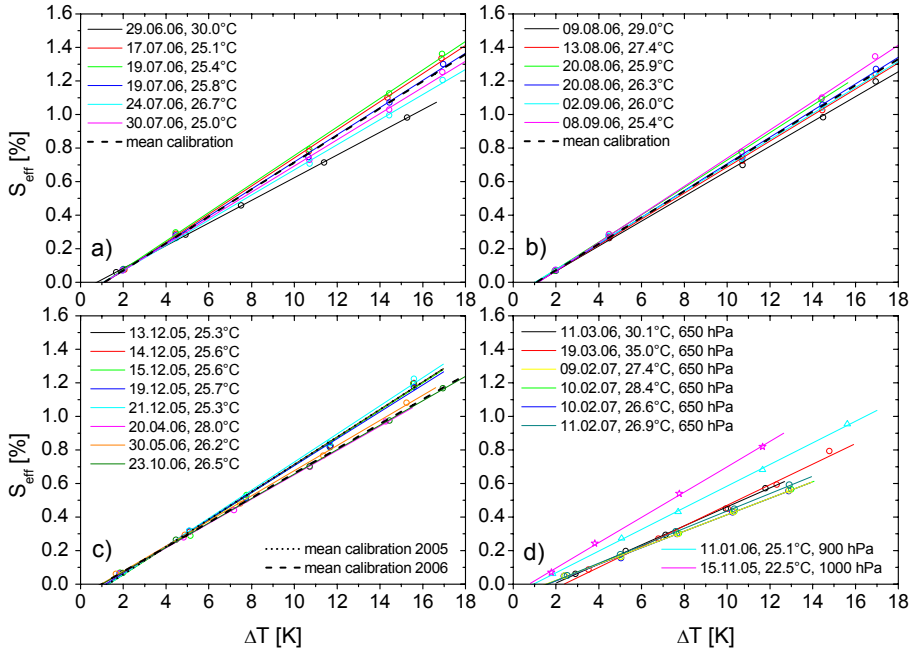

Fig. 4. Measured (symbols) and fitted (solid lines) calibration lines obtained from field and laboratory experiments with ammonium sulfate aerosol at different CCNC column top temperatures (T_1) and different locations: **(a)** field campaign in Guangzhou, China; **(b)** field campaign in Beijing, China; **(c)** laboratory measurements in Mainz, Germany; **(d)** field campaigns at the mountain stations Hohenpeissenberg, Germany (900 hPa) and Jungfraujoch, Switzerland (650 hPa) and laboratory measurement in Leipzig, Germany (1000 hPa). The CCNC was operated at Q=0.5 L min^{-1} and p≈1020 hPa unless mentioned otherwise. The dotted and dashed black lines are mean calibration lines (see text).

ACPD
7, 8193–8260, 2007

EGU

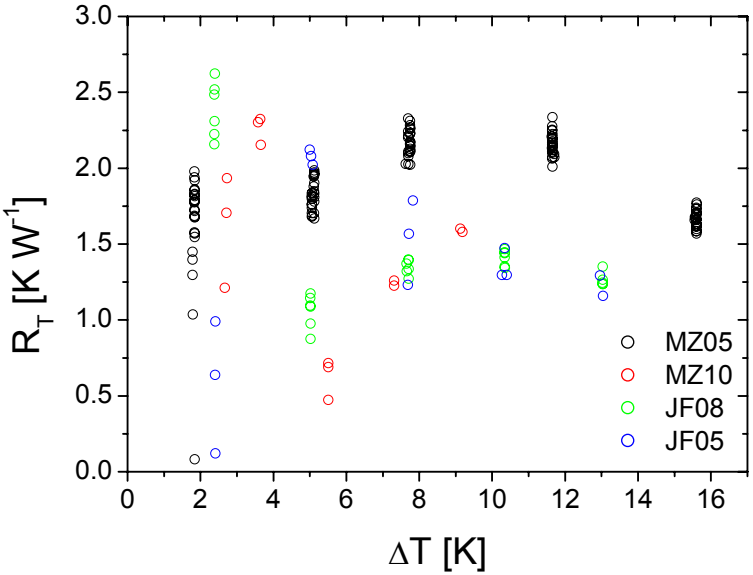

Fig. 5. Thermal resistance derived from four CCNC calibration experiments with ammonium sulfate aerosol at different pressures and flow rates (MZ05, MZ10, JF08, JF05, cf. Table 7) by fitting the CCNC flow model of Lance et al., 2006.

ACPD
7, 8193–8260, 2007

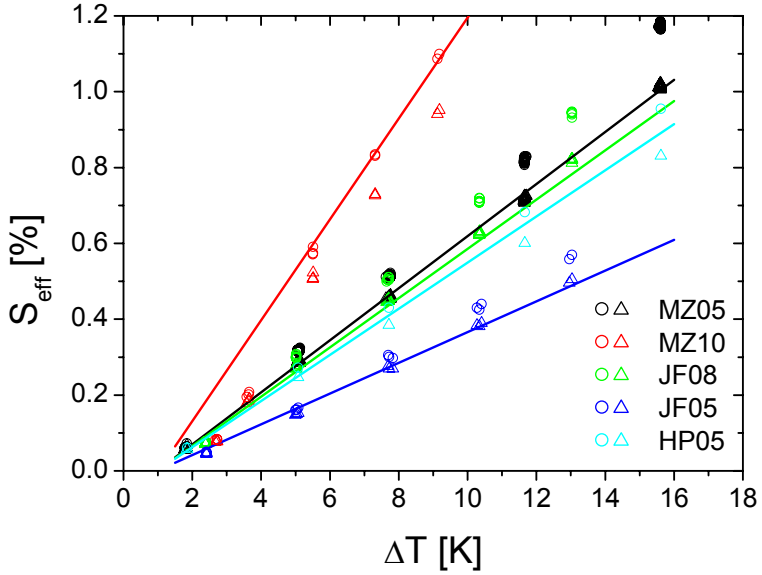

Fig. 6. Measured and modeled CCNC calibration lines obtained with ammonium sulfate aerosol under different operating conditions as detailed in Table 7. The triangles are the effective supersaturation values calculated from measured D_{50} using the Köhler model VH4.3 as used by Lance et al. (2006), and the lines are the corresponding flow model results. The circles are S_{eff} values calculated from measured D_{50} using the Köhler model VH4.1, as generally applied for ammonium sulfate in this study.

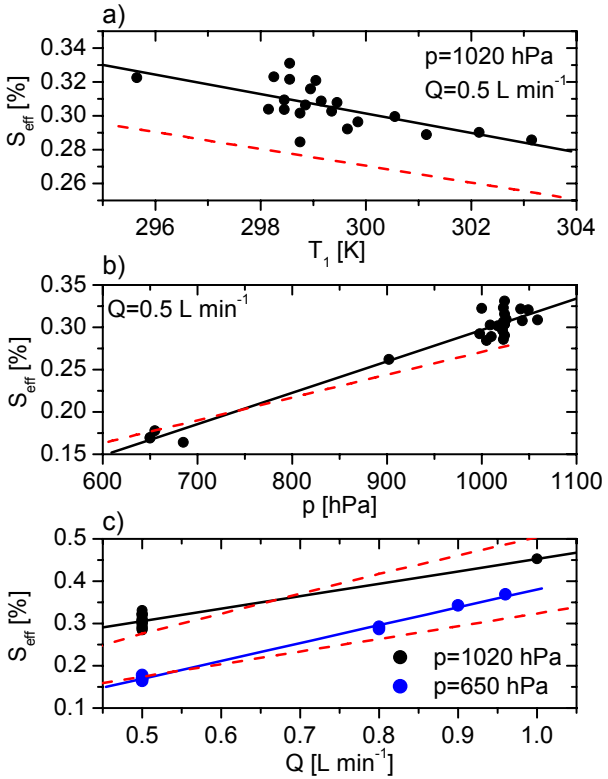

Fig. 7. Dependency of the effective supersaturation in the CCNC on **(a)** T_1, **(b)** pressure (p), **(c)** flow rate (Q). The data points are S_{eff} values calculated from all recorded ammonium sulfate calibration lines (Fig. 4) at ΔT=5 K. The solid lines are linear fits to the data points and the dashed lines are the S_{eff} values predicted by the CCNC flow model with R_T=1.78 K W^{-1}.

ACPD
7, 8193–8260, 2007

EGU

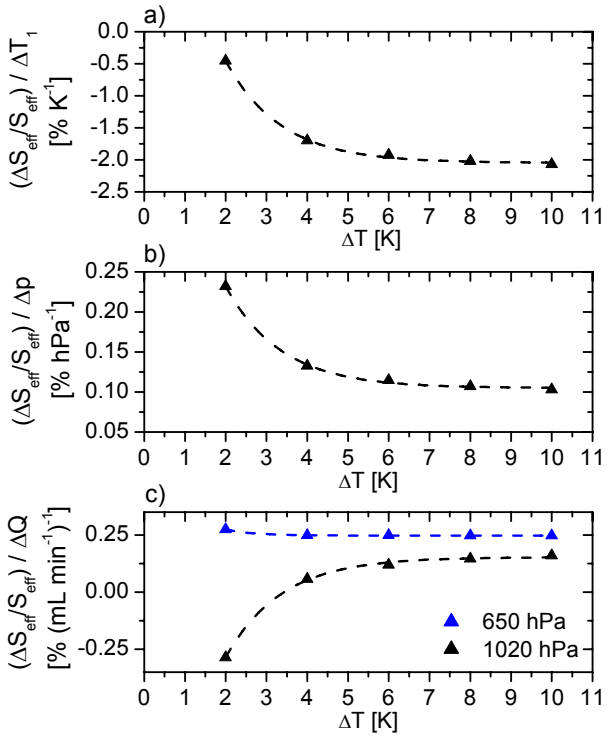

Fig. 8. Dependence of effective supersaturation on temperature (T_1), pressure (p), and flow rate (Q) in the CCNC averaged over all calibration experiments with ammonium sulfate aerosol. Every data point corresponds to the slope of a linear fit to all values of $\Delta S_{eff}/S_{eff}$ at a given ΔT plotted against T_1, p, or Q, respectively. $\Delta S_{eff}/S_{eff}$ is the relative deviation between S_{eff} from an individual calibration line and the mean value of S_{eff} for all calibrations performed at Q=0.5 L min^{-1} and p≈1020 hPa (black triangles) or 650 hPa (blue triangles), respectively. The dashed lines are first-order exponential decay fit functions.

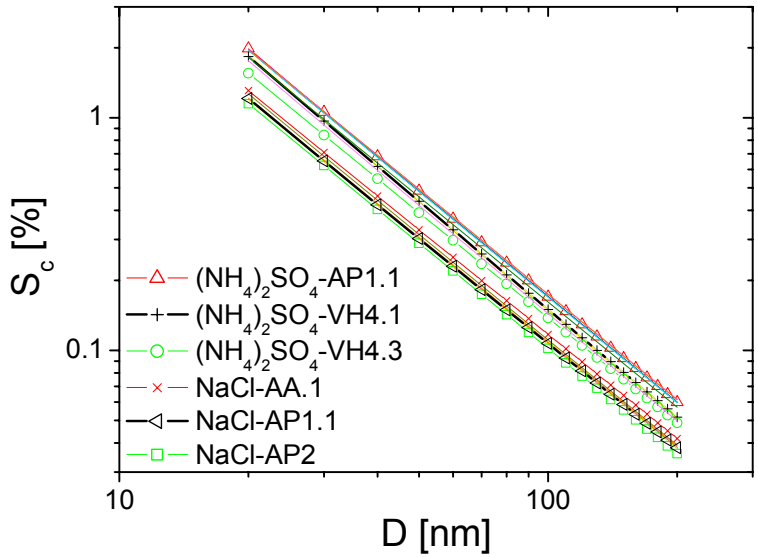

Fig. 9. Critical supersaturations (S_c) calculated for ammonium sulfate and sodium chloride particles with dry particle diameters (D) in the range of 20–200 nm using different Köhler model approaches as outlined in Table 5. All models are represented by lines; selected models with high, intermediate and low S_c values are additionally marked by symbols. For $(NH_4)_2SO_4$ we assumed D_s=D; for NaCl, D_s was obtained from Eq. (29) assuming cubic particle shape.

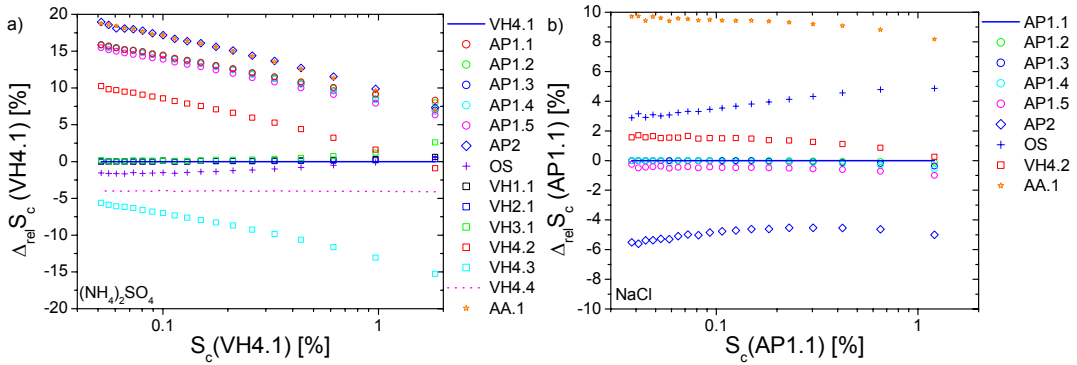

Fig. 10. Relative deviations of S_c values calculated with different Köhler models relative to the VH4.1 model for ammonium sulfate **(a)** and relative to the AP1.1 model for sodium chloride **(b)**.

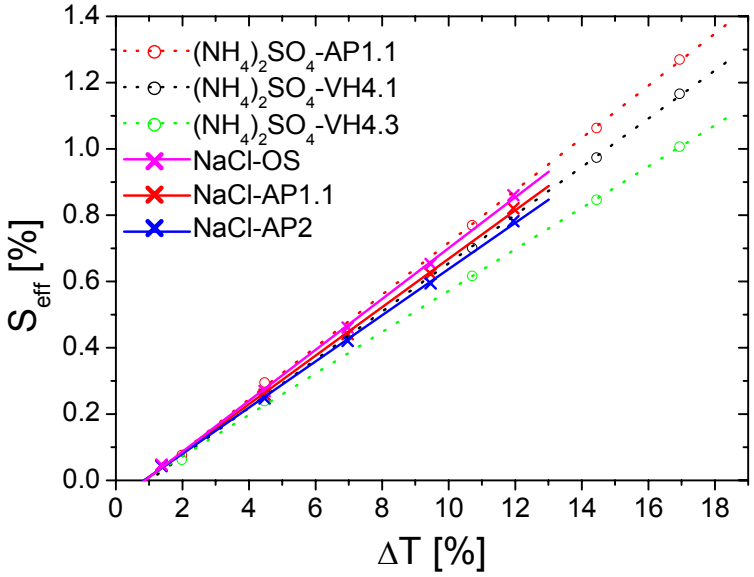

Fig. 11. Calibration lines of effective supersaturation (S_{eff}) vs. temperature difference (ΔT) obtained from one experiment with ammonium sulfate and one experiment with sodium chloride particles under equal conditions. The data points were calculated from measured D_{50} using different Köhler models; the lines are linear fits. Note that $(NH_4)_2SO_4$-AP1.1 is near-identical to $(NH_4)_2SO_4$-AP2.

ACPD
7, 8193–8260, 2007